PHYSICAL REVIEW D **89,** 094024 (2014)

Resonance effects in pion and kaon decay constants

Zhi-Hui Guo[1,*] and Juan José Sanz-Cillero[2,†]

[1]*Department of Physics, Hebei Normal University, 050024 Shijiazhuang, People's Republic of China and State Key Laboratory of Theoretical Physics, Institute of Theoretical Physics, Chinese Academy of Sciences, Beijing 100190, People's Republic of China*

[2]*Departamento de Física Teórica and Instituto de Física Teórica, IFT-UAM/CSIC, Universidad Autónoma de Madrid, Cantoblanco, 28049 Madrid, Spain*

(Received 10 March 2014; published 23 May 2014)

In this article we study the impact of the lightest vector and scalar resonance multiplets in the pion and kaon decay constants up to next-to-leading order in the $1/N_C$ expansion, i.e., up to the one-loop level. The F_π and F_K predictions obtained within the framework of resonance chiral theory are confronted with lattice simulation data. The vector loops (and the $\rho-\pi\pi$ coupling G_V in particular) are found to play a crucial role in the determination of the chiral perturbation theory couplings L_4 and L_5 at next-to-leading order in $1/N_C$. Puzzling, values of $G_V \lesssim 40$ MeV seem to be necessary to agree with current phenomenological results for L_4 and L_5. Conversely, a value of $G_V \gtrsim 60$ MeV compatible with standard $\rho-\pi\pi$ determinations turns these chiral couplings negative. However, in spite of the strong anti-correlation with L_4, the $SU(3)$ chiral coupling F_0 remains stable all the time and stays within the range $78 \sim 86$ MeV when G_V is varied in a wide range, from 40 up to 70 MeV. Finally, we would like to remark that the leading order expressions used in this article for the $\eta-\eta'$ mixing, mass splitting of the vector multiplet masses and the quark mass dependence of the $\rho(770)$ mass are found in reasonable agreement with the lattice data.

DOI: 10.1103/PhysRevD.89.094024 PACS numbers: 12.39.Fe, 14.40.Be, 11.15.Pg, 12.38.Gc

I. INTRODUCTION

The decay constants of the light pseudo Nambu-Goldstone bosons (pNGB) π and K are important quantities in particle physics. Their precise determinations are crucial for the extraction of the Cabibbo-Kobayashi-Maskawa matrix elements V_{ud} and V_{us} and for beyond standard model physics searches in the flavor sector [1,2]. They are one of the fundamental parameters in chiral perturbation theory (χPT), the effective field theory (EFT) of quantum chromodynamics (QCD) that describes the low-energy interactions between the pNGB (π, K, η) from the spontaneous chiral symmetry breaking [3,4]. In fact, these two decay constants F_π and F_K have been widely studied in χPT phenomenology [4,5] and lattice simulations [1,6]. However due to the rapid proliferation of the number of unknown low energy constants (LECs) at $\mathcal{O}(p^6)$, it is rather difficult to extract a definitive conclusion on the values of $\mathcal{O}(p^4)$ LECs and the $\mathcal{O}(p^2)$ coupling F_0 [1,5].

In spite of important progresses in the last years, lattice simulations usually compute the pNGB decay constants for values of the quark masses m_q heavier than the physical ones, in order to optimize computer resources. This worsens the convergence of the χPT series and higher chiral orders must be accounted and resummed in an appropriate way. However, apart from the chiral log behavior at small quark masses, these observables show an almost linear dependence on m_q, without any significant logarithmic behavior that one would expect from hadronic loop contributions. The inclusion of resonances within a chiral invariant framework, resonance chiral theory (RχT) [7], is expected to extend the applicability energy region of χPT up to some higher scale and explain this feature. The $1/N_C$ expansion [8], with N_C the numbers of colors in QCD, is taken as a guiding principle in RχT to sort out the various contributions, being hadronic loops suppressed by $1/N_C$. Indeed, at leading order (LO) in $1/N_C$, RχT predicts an almost linear m_q dependence for the decay constants with a slope given by the lightest scalar resonance mass [9], with fit value $M_S = 1049 \pm 25$ MeV: the same scalar resonance that mediates the scalar form factor into two pNGB at tree level also rules the quark mass corrections in the weak pNGB decay through an axial-vector current.

In the present work, we calculate the pion and kaon decay constants up to next-to-leading order (NLO) in $1/N_C$ within RχT, i.e., up to the one-loop level, continuing a series of previous NLO computations in this work line [10–14]. We hope in this way to properly incorporate the small m_q chiral log behavior without spoiling the roughly linear dependence found at large N_C [9]. This will allow us to match $SU(3)$ χPT at $\mathcal{O}(p^4)$ recovering the right renormalization scale dependence of the relevant LECs, $L_4(\mu)$ and $L_5(\mu)$. These theoretical predictions from RχT will be then confronted with the lattice results for F_π, F_K [15–18] and F_K/F_π [19].

The impact of meson resonances on the pNGB decay constants has not been thoroughly discussed in previous

*zhguo@mail.hebtu.edu.cn
†juanj.sanz@uam.es

literature. The only other one-loop attempt was carried out in the $SU(2)$ case and incorporated only the lightest scalar [20]. In this work we discuss the $SU(3)$ chiral dynamics and the effect of vector loops, in addition to the scalar ones. The outcomes in the present article are not expected to provide an improved version of the already very precise χPT computations present in the market, which are known now up to next-to-next-to-leading order (NNLO) in the chiral expansion [21,22] and incorporate specific lattice simulation subtleties (twisted boundary conditions [23], finite volume effects [24], etc.). The central aim of this article is to show how it is possible to study the dynamics of the lightest resonances through the analysis of these observables in the lattice. In particular we will see that the vector resonance loops (and more precisely the $\rho-\pi\pi$ coupling G_V) play an important role in the analysis and will be crucial for the final values of the χPT LECs F_0, L_4, and L_5.

The article is organized as follows: in Sec. II we introduce theoretical setup and the LO and NLO RχT Lagrangian. In Sec. III we perform the NLO computation in RχT, renormalization and matching between RχT and χPT. The fit to lattice data and the phenomenological discussions are carried out in Sec. IV. We finally provide the conclusions in Sec. V, relegating the most technical details to the Appendices.

II. RELEVANT RχT LAGRANGIAN

A. RχT building blocks

We will use the exponential realization of the $U(3)_L \otimes U(3)_R/U(3)_V$ coset coordinates for the pNGB,

$$U = u^2 = e^{i\frac{\sqrt{2}\phi}{F_0}}, \qquad D_\mu U = \partial_\mu U - i r_\mu U + i U \ell_\mu, \quad (1)$$

where the covariant derivative $D_\mu U$ incorporates the right and left external sources, respectively, r_μ and ℓ_μ, in such a way that it transforms in the same way as U under local chiral transformations [4]:

$$U \longrightarrow g_R U g_L^\dagger, \qquad u \longrightarrow g_R u h^\dagger = h u g_L^\dagger, \quad (2)$$

with the compensating transformation $h(\phi, g_R, g_L)$ [7]. Thus, the covariant derivative in Eq. (1) transforms in the form $(D_\mu U) \longrightarrow g_R (D_\mu U) g_L^\dagger$.

The pNGB octet plus the singlet η_1 are given by the matrix,

$$\phi = \sum_{a=0}^{8} \phi^a \frac{\lambda^a}{\sqrt{2}} = \begin{pmatrix} \frac{1}{\sqrt{2}}\pi^0 + \frac{1}{\sqrt{6}}\eta_8 + \frac{1}{\sqrt{3}}\eta_1 & \pi^+ & K^+ \\ \pi^- & \frac{-1}{\sqrt{2}}\pi^0 + \frac{1}{\sqrt{6}}\eta_8 + \frac{1}{\sqrt{3}}\eta_1 & K^0 \\ K^- & \bar{K}^0 & \frac{-2}{\sqrt{6}}\eta_8 + \frac{1}{\sqrt{3}}\eta_1 \end{pmatrix}. \quad (3)$$

Notice that due to the inclusion of the singlet η_1, the standard chiral counting from $SU(3)$–χPT given by an expansion in powers of the momenta and the pNGB masses does not work any more, since the mass of η_1 does not vanish in the chiral limit ($m_{\eta_1} \to M_0 \simeq 850$ MeV when $m_q \to 0$ [25]). However, by introducing $1/N_C$ as a third expansion parameter, it is still possible to establish a consistent power counting system for $U(3)$–χPT [26], which includes the singlet η_1 as a dynamical degree of freedom (d.o.f).

The basic building blocks of the meson theory read

$$u_\mu = i u^\dagger D_\mu U u^\dagger = i\{u^\dagger(\partial_\mu - i r_\mu)u - u(\partial_\mu - i\ell_\mu)u^\dagger\},$$
$$\chi_\pm = u^\dagger \chi u^\dagger \pm u \chi^\dagger u, \qquad f_\pm^{\mu\nu} = u F_L^{\mu\nu} u^\dagger \pm u^\dagger F_R^{\mu\nu} u, \quad (4)$$

where $\chi = 2B(s+ip)$ includes the scalar (s) and pseudoscalar (p) external sources, and $F_L^{\mu\nu}$ and $F_R^{\mu\nu}$ are, respectively, the left and right field-strength tensors [4]. All the referred tensors $X = u_\mu, \chi_\pm, f_\pm^{\mu\nu}$ transform under chiral transformations as

$$X \longrightarrow h X h^\dagger. \quad (5)$$

We will also make use of the covariant derivative for this type of object,

$$\nabla_\mu X = \partial_\mu X + [\Gamma_\mu, X],$$
$$\Gamma_\mu = \frac{1}{2}[u^\dagger(\partial_\mu - i r_\mu)u + u(\partial_\mu - i\ell_\mu)u^\dagger]. \quad (6)$$

In our analysis we will study the impact of the lightest $U(3)$ nonets of vector and scalar resonances surviving at large N_C. We will employ a representation of the resonance fields $R = V, S$ such that they transform in the way $R \longrightarrow h R h^\dagger$ in Eq. (5) under chiral transformations [7]. The flavor assignment for the scalar and vector resonances is similar to that in Eq. (3):

$$S = \begin{pmatrix} \frac{a_0^0}{\sqrt{2}} + \frac{\sigma_8}{\sqrt{6}} + \frac{\sigma_1}{\sqrt{3}} & a_0^+ & \kappa^+ \\ a_0^- & -\frac{a_0^0}{\sqrt{2}} + \frac{\sigma_8}{\sqrt{6}} + \frac{\sigma_1}{\sqrt{3}} & \kappa^0 \\ \kappa^- & \bar{\kappa}^0 & -\frac{2\sigma_8}{\sqrt{6}} + \frac{\sigma_1}{\sqrt{3}} \end{pmatrix}, \quad (7)$$

$$V_{\mu\nu} = \begin{pmatrix} \frac{\rho_0}{\sqrt{2}} + \frac{1}{\sqrt{6}}\omega_8 + \frac{1}{\sqrt{3}}\omega_1 & \rho^+ & K^{*+} \\ \rho^- & -\frac{\rho_0}{\sqrt{2}} + \frac{1}{\sqrt{6}}\omega_8 + \frac{1}{\sqrt{3}}\omega_1 & K^{*0} \\ K^{*-} & \bar{K}^{*0} & -\frac{2}{\sqrt{6}}\omega_8 + \frac{1}{\sqrt{3}}\omega_1 \end{pmatrix}_{\mu\nu}. \quad (8)$$

The vector resonances are described here in the antisymmetric tensor formalism through the $V_{\mu\nu}$ fields [7]. In later discussions, we will consider the ideal $I = 0$ resonance mixings

$$\sigma_8 = \sqrt{\frac{1}{3}}\sigma - \sqrt{\frac{2}{3}}\sigma', \qquad \sigma_1 = \sqrt{\frac{2}{3}}\sigma + \sqrt{\frac{1}{3}}\sigma', \quad (9)$$

$$\omega_8 = \sqrt{\frac{2}{3}}\phi + \sqrt{\frac{1}{3}}\omega, \qquad \omega_1 = \sqrt{\frac{2}{3}}\omega - \sqrt{\frac{1}{3}}\phi, \quad (10)$$

for the octet and singlet scalar and vector resonances, which leads to two different types of isoscalar resonances $R^{\bar{u}u+\bar{d}d}_{I=0}$ and $R^{\bar{s}s}_{I=0}$ in the quark flavor basis. This pattern was found to provide an excellent phenomenological description for the vector resonance multiplets [27]. We would like to stress that the resonances incorporated in our framework are the ones surviving at large N_C. The lowest multiplet of vector resonances $(\rho, K^*, \omega, \phi)$ behaves very approximately like a standard $\bar{q}q$ resonance, with a mass that tends to a constant and a width decreasing like $1/N_C$ when $N_C \to \infty$ [28–31]. This allows us to build a one-to-one correspondence between the physical vector resonances and those surviving at large N_C. On the other hand, the nature of the light scalar resonances, such as $f_0(500)$,$f_0(980)$, $K_0^*(800)$, etc., is still unclear and various descriptions are proposed by different groups: meson-meson molecular, tetraquark, standard $\bar{q}q$ with a strong pion cloud, etc. As a result of this, their N_C behavior is also under debate [28,29,31–34]. Though the N_C trajectories of the scalar resonances reported by different groups diverge from each other, surprisingly there is one common feature from Refs. [28,29,31–33]: a scalar resonance with mass around 1 GeV appears at large N_C. Based on these results and the success of this hypothesis in previous analyses [10,11,27], we will assume in the present article the existence of a large–N_C scalar nonet with a bare mass around 1 GeV.

On the other hand, the situation is slightly more cumbersome for η_8 and η_1 and one needs to consider the mixing

$$\eta_8 = c_\theta \eta + s_\theta \eta', \qquad \eta_1 = -s_\theta \eta + c_\theta \eta', \quad (11)$$

with $c_\theta = \cos\theta$ and $s_\theta = \sin\theta$. Phenomenologically, one has $\theta = (-13.3 \pm 0.5)^\circ$ in QCD [35], far away from the ideal mixing $\theta = -\arcsin\sqrt{\frac{2}{3}} \simeq -55^\circ$. We will see that only the leading order mixing will be relevant in the present analysis of F_π and F_K.[1] In the loop calculation, it is convenient to use the physical states η and η', instead of the flavor eigenstates η_1 and η_8. The reason is that the mixing between η_1 and η_8 is proportional to $m_K^2 - m_\pi^2$, which is formally the same order as the masses of η_1 and η_8. The insertion of the η_1 and η_8 mixing in the chiral loops will not increase the $1/N_C$ order of the loop diagrams. This makes the loop calculation technically complicated. However, as already noticed in Refs. [29–31], one can easily avoid the complication in the loop computation by expressing the Lagrangian in terms of the η and η' states resulting from the diagonalization of η_1 and η_8 at leading order. In addition, the effect of the mixing is less and less important in the lattice simulations as m_π increases and approaches m_K, making subleading uncertainties in the mixing even more suppressed. Therefore, in the following discussion, we will always calculate the loop diagrams in terms of η and η' states, instead of η_1 and η_8. Further details on the η–η' mixing are relegated to Appendix B.

B. LO Lagrangian

In general, one can classify the RχT operators in the Lagrangian according to the number of resonance fields in the form

$$\mathcal{L}_{\mathrm{R}\chi\mathrm{T}} = \mathcal{L}_G + \sum_R \mathcal{L}_R + \cdots \quad (12)$$

where the operators in $\mathcal{L}_G$ only contains pNGB and external sources, the $\mathcal{L}_R$ terms have one resonance field in addition to possible pNGB and external auxiliary fields, and the dots stand for operators with two or more resonances.

We focus first on the $\mathcal{L}_G$ part of the RχT Lagrangian. Since we will later incorporate the lightest $U(3)$ nonet of hadronic resonances and we are working within a large–N_C framework, our theory will be based on the $U(3)_L \otimes U(3)_R$ symmetry and, in addition to the two usual $\mathcal{O}(p^2)$ operators from $SU(3)$ χPT, we will also need to consider the singlet η_1 mass term:

$$\mathcal{L}_G^{\mathrm{LO}} = \frac{\tilde{F}^2}{4}\langle u_\mu u^\mu \rangle + \frac{\hat{F}^2}{4}\langle \chi_+ \rangle + \frac{F_0^2}{3}M_0^2 \ln^2 \det u, \quad (13)$$

[1]This is because η and η' only enter the pion and kaon decay constants through the chiral loops. Subleading contributions to the mixing will be neglected as they will enter as corrections in one-loop suppressed diagrams in the pNGB decay.

where $\langle\ldots\rangle$ stands for the trace in flavor space. The last operator in the right-hand side (r.h.s.) of Eq. (13) is generated by the $U_A(1)$ anomaly and gives mass to the singlet η_1. On the contrary to χPT, in RχT one generates ultraviolet (UV) divergences which require the first two terms in the r.h.s of Eq. (13) to fulfill the renormalization of the resonance loops [10,36]. Notice that a different coupling notation $\alpha_1 = \tilde{F}^2/4$ and $\alpha_2 = \hat{F}^2/4$ is used in Ref. [36]. As $\tilde{F}$ and $\hat{F}$ describe the chiral limit pNGB decay constant from an axial-vector current and a pseudoscalar density, respectively, one has that $\lim_{N_C\to\infty}\tilde{F}/F_0 = \lim_{N_C\to\infty}\hat{F}/F_0 = 1$. F_0 stands for the $n_f = 3$ decay constant of the pNGB octet in the chiral limit. The parameter B in χ_+ from Eq. (4) is connected with the quark condensate through $\langle 0|\bar{q}^i q^j|0\rangle = -F_0^2 B\delta^{ij}$ in the same limit. The explicit chiral symmetry breaking is realized by setting the scalar external source field to $s = \mathrm{Diag}(m_u, m_d, m_s)$, being m_q the light quark masses. We will consider the isospin limit all along the work, i.e., we will take $m_u = m_d$ (denoted just as $m_{u/d}$) and neglect any electromagnetic correction.

In order to account for the resonance effects, we consider the minimal resonance operators in the leading order RχT Lagrangian [7]

$$\mathcal{L}_V = \frac{F_V}{2\sqrt{2}}\langle V_{\mu\nu} f_+^{\mu\nu}\rangle + \frac{iG_V}{2\sqrt{2}}\langle V_{\mu\nu}[u^\mu, u^\nu]\rangle, \tag{14}$$

$$\mathcal{L}_S = c_d\langle S u_\mu u^\mu\rangle + c_m\langle S\chi_+\rangle. \tag{15}$$

In general, one could consider the resonance operators of the type $\langle R\chi^{(n\geq 4)}(\phi)\rangle$, with the chiral tensor $\chi^{(n)}(\phi)$ only including the pNGB and external fields and n standing for the chiral order of this chiral tensor. The resonance operators in the previous two equations are of type $\langle R\chi^{(2)}(\phi)\rangle$. Operators with higher values of n tend to violate the high-energy asymptotic behavior dictated by QCD for form factors and Green functions. Likewise, by means of meson field redefinitions it is possible to trade some resonance operators by other terms with a lower number of derivatives and operators without resonance fields [10,13,37,38]. As a result of this, only the lowest order chiral tensors are typically employed to build the operators of the leading order RχT Lagrangian. We will follow this heuristic rule in the present work. Nevertheless, we remind the reader that the truncation of the infinite tower of large-N_C resonances introduces in general a theoretical uncertainty in the determinations, which will be neglected in our computation. Considering only the lightest resonance multiplets may lead to some issues with the short-distance constraints and the low-energy predictions when a broader and broader set of observables is analyzed [39].

In Ref. [29], two additional resonance operators were taken into account [the last two terms in Eq. (5) of the previous reference]. These two terms are $1/N_C$ suppressed with respect to the RχT operator in Eq. (15). They happen to be irrelevant for our current study up to NLO in $1/N_C$ since they involve at least one η or η' fields. As we already mentioned previously, η and η' only enter our calculation through chiral loops and the two additional operators in Ref. [29] would contribute to F_π and F_K at next-to-next-to-leading order in $1/N_C$. Thus, the one-loop calculation at NLO in $1/N_C$ only requires the consideration of the LO resonance operators like those in Eqs. (14) and (15).

The corresponding kinematical terms for resonance fields are [7]

$$\mathcal{L}^V_{\mathrm{kin}} = -\frac{1}{2}\langle\nabla^\lambda V_{\lambda\mu}\nabla_\nu V^{\nu\mu} - \frac{1}{2}\bar{M}_V^2 V_{\mu\nu}V^{\mu\nu}\rangle, \tag{16}$$

$$\mathcal{L}^S_{\mathrm{kin}} = \frac{1}{2}\langle\nabla^\mu S\nabla_\mu S - \bar{M}_S^2 S^2\rangle. \tag{17}$$

In our current work, we also incorporate the light quark mass corrections to the resonance masses and in the large N_C limit this effect is governed by the operators [40][2]

$$\mathcal{L}^{\mathrm{split}}_{RR} = e_m^S\langle SS\chi_+\rangle - \frac{1}{2}e_m^V\langle V_{\mu\nu}V^{\mu\nu}\chi_+\rangle. \tag{18}$$

In the notation of Ref. [41] these two couplings would be given by $e_m^S = \lambda_3^{SS}$ and $e_m^V = -2\lambda_6^{VV}$. If no further bilinear resonance term is included in the Lagrangian, one has an ideal mixing for the two $I = 0$ resonances in the nonet and a mass splitting pattern of the form

$$\begin{aligned}(M^{\bar{u}u+\bar{d}d}_{I=0})^2 = M^2_{I=1} &= \bar{M}_R^2 - 4e_m^R m_\pi^2,\\ M^2_{I=\frac{1}{2}} &= \bar{M}_R^2 - 4e_m^R m_K^2,\\ M^{(\bar{s}s)^2}_{I=0} &= \bar{M}_R^2 - 4e_m^R(2m_K^2 - m_\pi^2),\end{aligned} \tag{19}$$

with $\bar{M}_R$ the resonance mass in chiral limit. Notice that in the following we will use the notations M_S and M_V for the masses of scalar and vector multiplets in chiral limit, respectively.

At large N_C, the coupling of the LO Lagrangian scale like $F_0, \tilde{F}, \hat{F}, G_V, c_d, c_m = \mathcal{O}(N_C^{\frac{1}{2}})$ and the masses of the mesons considered here behave like $m_\phi, M_R, = \mathcal{O}(N_C^0)$, with the splitting parameter $e_m^R = \mathcal{O}(N_C^0).M_0$, which is the chiral limit of the η_1 mass, is formally $\mathcal{O}(N_C^{-1})$, although numerically it provides a sizable contribution to the $\eta - \eta'$ mixing that needs to be taken into account in order to properly reproduce their masses and mixing angles. More details can be found in Appendix B.

[2]Notice that the different canonical normalization of the scalar and vector mass terms is responsible for the $(-\frac{1}{2})$ factor in front of the vector splitting operator.

C. NLO RχT Lagrangian

In general, one should also take into account local operators with a higher number of derivatives [e.g., $\mathcal{O}(p^4)$] in RχT. In particular one might consider operators composed only of pNGB and external fields. Notice that these terms of the RχT Lagrangian are different from those in χPT, as they are two different quantum field theories with different particle content.

Based on phenomenological analyses and short-distance constraints it is well known that the leading parts of the χPT LECs are found to be saturated by the lowest resonances at large N_C [7,42]. The operators of RχT without resonances of $\mathcal{O}(p^{d\geq 4})$ can be regarded as $1/N_C$ suppressed residues, absent when $N_C \to \infty$. Nonetheless the resonance saturation scale cannot be determined at large N_C as this is a NLO effect in $1/N_C$. Since in this work we perform the discussion at the NLO of $1/N_C$, we will include these residual RχT operators without resonance fields, which start being relevant at NLO in $1/N_C$.

The pertinent $\mathcal{O}(p^4)$ operators in our study are [4]

$$\begin{aligned}\mathcal{L}_G^{\rm NLO} &= \tilde{L}_4\langle u_\mu u^\mu\rangle\langle\chi_+\rangle + \tilde{L}_5\langle u_\mu u^\mu\chi_+\rangle \\ &+ \tilde{L}_6\langle\chi_+\rangle\langle\chi_+\rangle + \tilde{L}_7\langle\chi_-\rangle\langle\chi_-\rangle + \frac{\tilde{L}_8}{2}\langle\chi_+\chi_+ + \chi_-\chi_-\rangle \\ &+ i\tilde{L}_{11}\left\langle\chi_-\left(\nabla_\mu u^\mu - \frac{i}{2}\chi_- + \frac{i}{2n_f}\langle\chi_-\rangle\right)\right\rangle \\ &- \tilde{L}_{12}\left\langle\left(\nabla_\mu u^\mu - \frac{i}{2}\chi_- + \frac{i}{2n_f}\langle\chi_-\rangle\right)^2\right\rangle, \end{aligned} \tag{20}$$

where $n_f = 3$ and the tilde is introduced to distinguish the RχT couplings from the χPT LECs L_j. The set of $\mathcal{L}_G^{\rm NLO}$ couplings scale like $\tilde{L}_j = \mathcal{O}(N_C^0)$ within the $1/N_C$ expansion and are suppressed with respect to the $\mathcal{O}(p^4)$ LECs, which behave like $L_j = \mathcal{O}(N_C)$. The parameters $\tilde{L}_{11}$ and $\tilde{L}_{12}$ will not appear in the final results for F_π and F_K, as their contributions in the matrix element of the axial-vector current will be canceled out by the wave function renormalization constant of the pNGB.

One should notice that the chiral operators in the previous equation are exactly the same as in χPT, but the coefficients can be completely different. In order to extract the low-energy EFT couplings one needs to integrate out the heavy d.o.f in the RχT action. At tree level, the χPT LECs get two kinds of contributions: one comes directly from the $\tilde{L}_i$ operators with only pNGB and external sources; the other, $L_i^{\rm Res}$, comes from the tree-level resonance exchanges when $p^2 \ll M_R^2$. Hence, the relations between the couplings in RχT and those in χPT are given by [7,42,43]

$$L_i^{\chi\rm PT} = L_i^{\rm Res} + \tilde{L}_i. \tag{21}$$

From now on, in order to avoid any possible confusion we will explicitly write the superscript χPT when referring to the chiral LECs. The large–N_C resonance contributions to the $\mathcal{O}(p^4)$ LECs were computed in Ref. [7] by integrating out the resonance in the RχT generating functional, yielding

$$L_4^{\rm Res}|_{N_C\to\infty} = 0, \quad L_5^{\rm Res}|_{N_C\to\infty} = \left.\frac{c_d c_m}{M_S^2}\right|_{N_C\to\infty} = \frac{F_0^2}{4M_S^2}, \tag{22}$$

where in the last equality we have used the high-energy scalar form-factor constraint $4c_d c_m = F_0^2$ [44]. Other couplings in Eq. (20) will be irrelevant to our final results for the pion and kaon decay constants.

D. Scalar resonance tadpole and the field redefinition

Before stepping into the detailed calculation, we point out a subtlety about the treatment of the scalar resonance operators in Eq. (15). The operator with c_m coupling in this equation leads to a term that couples the isoscalar scalar resonances S_8 and S_1 to the vacuum. In other words, it generates a scalar resonance tadpole proportional to the quark masses. Though it is not a problem to perform the calculations with such tadpole effects, it can be rather cumbersome. We find it is convenient to eliminate it at the Lagrangian level. This will greatly simplify the calculation when the resonances enter the loops. Nonetheless, at tree level it does not make much difference to eliminate the tadpole at the Lagrangian level [9] or just to calculate perturbatively the tadpole diagrams [29–31].

In order to eliminate the scalar tadpole effects from the Lagrangian, we make the following field redefinition for the scalar resonances

$$S = \bar{S} + \frac{c_m}{M_S^2}\chi_+, \tag{23}$$

with $\bar{S}$ being the scalar resonance fields after the field redefinition. By substituting Eq. (23) into Eqs. (15) and (17), one has

$$\begin{aligned}\mathcal{L}_{\rm kin}^S + \mathcal{L}_S &= \frac{1}{2}\langle\nabla^\mu\bar{S}\nabla_\mu\bar{S} - M_S^2\bar{S}^2\rangle + c_d\langle\bar{S}u_\mu u^\mu\rangle \\ &+ \frac{c_m}{M_S^2}\langle\nabla_\mu\bar{S}\nabla^\mu\chi_+\rangle + \frac{c_d c_m}{M_S^2}\langle\chi_+ u_\mu u^\mu\rangle \\ &+ \frac{c_m^2}{2M_S^2}\langle\chi_+\chi_+\rangle + \frac{c_m^2}{2M_S^4}\langle\nabla_\mu\chi_+\nabla^\mu\chi_+\rangle. \end{aligned} \tag{24}$$

The first line has the same structure as the original Lagrangian with S replaced by $\bar{S}$ but with the corresponding tadpole operator $c_m\langle\bar{S}\chi_+\rangle$ absent. Instead, it has been traded out by the derivative term $\frac{c_m}{M_S^2}\langle\nabla_\mu\bar{S}\nabla^\mu\chi_+\rangle$ at the price of the extra operators in the second and third lines. We want to note that the last operator in Eq. (24) is not considered in the following discussion, as it corresponds to the set of

local $\mathcal{O}(p^6)$ operators without resonance fields and contributes to the decay constants at the order of m_q^2, which was neglected and discarded in the previous section. These kinds of contributions escape the control of the present analysis, as there are many other types of resonance operators (e.g., the previously mentioned $\langle S\chi^{(4)}(\phi)\rangle$ type) which would generate similar terms without resonances after the scalar field redefinition in Eq. (23) but were neglected here. The same applies to the resonance mass splitting Lagrangian $\mathcal{L}_{RR}^{\rm split}$ in Eq. (18): the scalar field redefinition in Eq. (23) generates extra splitting operators of order m_q^2 and m_q^3 which will be neglected in this work.

At NLO in $1/N_C$, the LO Lagrangian (15) induces a scalar resonance tadpole proportional to m_q^2 through a pNGB loop. In order to remove it one should perform another scalar field shift similar to Eq. (23) but of the form $\Delta S \sim \frac{c_j m_\phi^4}{16\pi^2 F_0^2 M_S^2}$, with $c_j = c_d, c_m$. This yields a contribution to the pNGB decay constants doubly suppressed, by m_ϕ^4 and $1/N_C$. Hence, following the previous considerations, we will neglect the one-loop tadpole effects.

Hence, after performing the shift in the scalar field worked out in this section, RχT contains operators without resonances in Eq. (24) with the same structure as the L_j ones in the $\mathcal{O}(p^4)$ χPT Lagrangian [4]. Combining Eqs. (20) and (24), we have the *effective* couplings in RχT

$$\tilde{\tilde{L}}_4 = \tilde{L}_4, \qquad \tilde{\tilde{L}}_5 = \frac{c_d c_m}{M_S^2} + \tilde{L}_5, \qquad \tilde{\tilde{L}}_8 = \frac{c_m^2}{2M_S^2} + \tilde{L}_8, \tag{25}$$

with the couplings of the remaining $\mathcal{O}(p^4)$ operators without resonances just given by $\tilde{\tilde{L}}_j = \tilde{L}_j$. In general the double-tilde notation will refer to the coupling of the Lagrangian operator after performing the scalar field shift in Eq. (23). It is easy to observe that at large N_C one recovers the RχT results in Eq. (22): $\tilde{\tilde{L}}_4$ and $\tilde{\tilde{L}}_5$ become equal to the $\mathcal{O}(p^4)$ LECs $L_4^{\chi PT}$ and $L_5^{\chi PT}$, respectively, as there is no other possible $\mathcal{O}(p^4)$ resonance contribution of this kind after performing the S–shift in Eq. (23). Though L_8 will not enter the discussion in the pion and kaon decay constants, for completeness we comment that our result in Eq. (25) is consistent with the scalar contributions in Ref. [7], as $\tilde{\tilde{L}}_8$ would become equal to $L_8^{\chi\rm PT}$ in the large–N_C limit.

III. THEORETICAL CALCULATION

A. Decay constants in RχT at NLO in $1/N_C$

The pNGB decay constant is defined through the matrix element of the axial-vector current of the light quarks

$$\langle\phi(p)|\bar{q}\gamma_\mu\gamma_5 u|0\rangle = -i\sqrt{2}F_\phi p_\mu, \quad \text{with} \quad \phi = \pi(K) \quad \text{for } q = d(s). \tag{26}$$

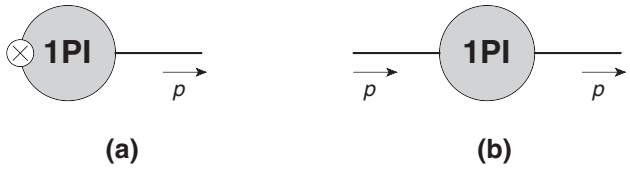

FIG. 1. Relevant vertex functions for the physical pNGB decay constant: (a) 1PI transitions between an axial-vector current and a bare pseudo-Goldstone field, determining $F_\phi^{\rm 1PI}$; (b) pNGB self-energy $-i\Sigma_\phi(p^2)$. The solid line stands for a pNGB ϕ, the crossed circle for an axial-vector current insertion, and the circle represents all possible 1PI topologies.

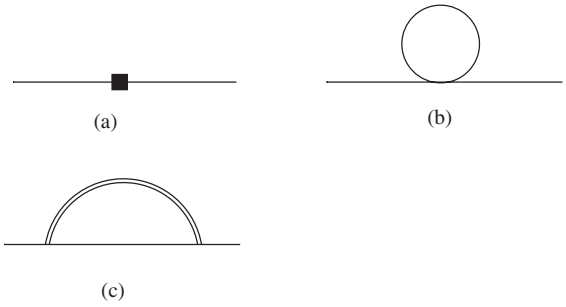

FIG. 2. Feynman diagrams of the pNGB self-energy. The single line corresponds to pNGB and the double line stands for a resonance state. The tree-level amplitude in diagram (a) can receive contributions both from the leading order Lagrangian in Eq. (13), the contact terms appearing in the second line of Eq. (24), and the $\mathcal{O}(p^4)$ Lagrangian in Eq. (20). The vertices in diagram (b) are from the leading order Lagrangian in Eq. (13) and the vertices in diagram (c) are from Eqs. (14),(15), and (24).

In order to study the pion and kaon axial decay constants at NLO of $1/N_C$, we need to calculate the one-loop diagrams with resonances running inside the loops and then perform the renormalization. If the scalar tadpole is conveniently canceled out in the way explained in Sec. II D, the renormalized matrix element that provides F_ϕ is then determined by the two 1-particle-irreducible (1PI) vertex functions depicted in Fig. 1. More explicitly, we plot in Figs. 2 and 3 the precise diagrams which will be relevant in our RχT computation of the pNGB decay constant up to NLO of $1/N_C$. Hence, the expression for the physical decay constant consists of two pieces

$$F_\phi = Z_\phi^{\frac{1}{2}} F_\phi^{\rm 1PI}, \tag{27}$$

where Z_ϕ stands for the wave-function renormalization constant of the pNGB given by $\phi^{(B)} = Z_\phi^{\frac{1}{2}}\phi^r$ ($\phi = \pi, K$) in the on-shell scheme (Fig. 1b) and $F_\phi^{\rm 1PI}$ denotes the contributions from 1PI topologies for the transition between an axial-vector current and a bare pNGB $\phi^{(B)}$ (Fig 1a). The wave-function renormalization constant $Z_\phi = 1 + \delta Z_\phi$ is related to the pNGB self-energy $\Sigma_\phi(p^2)$ through

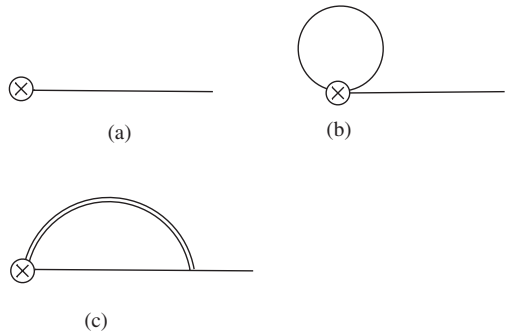

FIG. 3. Feynman diagrams of the pNGB axial-vector decay constant. The circled cross symbol corresponds to the axial-vector source. Similar to Fig. 2, diagram (a) can receive contributions from the leading order Lagrangian in Eq. (13), the contact terms appearing in the second line of Eq. (24), and the $\mathcal{O}(p^4)$ Lagrangian in Eq. (20). The vertices in diagram (b) are from the leading order Lagrangian in Eq. (13) and the vertices in diagram (c) are from Eqs. (14),(15), and (24).

$$Z_\phi = (1-\Sigma'_\phi)^{-1} = \left(1 - \left.\frac{d\Sigma_\phi(p^2)}{dp^2}\right|_{p^2=m_\phi^2}\right)^{-1}. \quad (28)$$

For convenience, we will explicitly separate the tree-level and one-loop contributions in RχT,

$$Z_\phi = \left(\frac{\tilde{F}^2}{F_0^2} + \frac{8\tilde{\tilde{L}}_4(2m_K^2+m_\pi^2)}{F_0^2} + \frac{8\tilde{\tilde{L}}_5 m_\phi^2}{F_0^2} + \frac{8\tilde{L}_{11}m_\phi^2}{F_0^2} - \Sigma'_{\phi,1\ell}\right)^{-1}, \quad (29)$$

$$\frac{F_\phi^{1\mathrm{PI}}}{F_0} = \frac{\tilde{F}^2}{F_0^2} + \frac{8\tilde{\tilde{L}}_4(2m_K^2+m_\pi^2)}{F_0^2} + \frac{8\tilde{\tilde{L}}_5 m_\phi^2}{F_0^2} + \frac{4\tilde{L}_{11}m_\phi^2}{F_0^2} + \frac{F_{\phi,1\ell}^{1\mathrm{PI}}}{F_0}, \quad (30)$$

with the corresponding one-loop corrections $\Sigma'_{\phi,1\ell}$ and $F_{\phi,1\ell}^{1\mathrm{PI}}$. This yields the physical decay constant given by

$$F_\phi = F_0\left(\frac{\tilde{F}}{F_0} + \frac{4\tilde{\tilde{L}}_4(2m_K^2+m_\pi^2)}{F_0^2} + \frac{4\tilde{\tilde{L}}_5 m_\phi^2}{F_0^2} + \frac{F_{\phi,1\ell}^{1\mathrm{PI}}}{F_0} + \frac{1}{2}\Sigma'_{\phi,1\ell}\right), \quad (31)$$

where $Z_\phi^{\frac{1}{2}}$ has been expanded in this expression, keeping just the linear contribution in δZ_ϕ and dropping other terms $\mathcal{O}((\delta Z_\phi)^2)$ or higher. In particular, we have used $\tilde{F}/F_0 = 1 + \mathcal{O}(N_C^{-1})$ and dropped terms $\mathcal{O}((\tilde{F}/F_0 - 1)^2)$. Notice that there is not a uniquely defined way of truncating the NNLO corrections: for instance, a slightly different numerical prediction is obtained if instead of the expression for F_ϕ in Eq. (31) one employs the NLO result for F_ϕ^2, dropping terms $\mathcal{O}((\delta Z_\phi)^2)$ or higher as we did in Eq. (31). The spurious coupling $\tilde{L}_{11}$ (corresponding to an operator proportional to the equations of motion [10]) then becomes canceled out and disappears from the physical observable.

Since we did not consider $\mathcal{O}(p^6)$ operators in the Lagrangian $\mathcal{L}_G^{\mathrm{LO}}$ in Eq. (13), we will neglect the terms $\mathcal{O}(\tilde{\tilde{L}}_{4,5}^2 m_\phi^4/F^4)$ in the decay constant in Eq. (31) which would arise from the expansion at that order of $Z_\phi^{\frac{1}{2}}$. In spite of having the same tree-level structure, in general the loop UV–divergences in Z_ϕ and $F_\phi^{1\mathrm{PI}}$, given respectively in Eqs. (29) and (30), are different. Thus, one must combine these two quantities into Eq. (31) in order to get a finite decay constant F_ϕ by means of the renormalization of $\tilde{F}$, $\tilde{\tilde{L}}_4$, and $\tilde{\tilde{L}}_5$.

In the $N_C \to \infty$ limit, the meson loops are absent and one has

$$\tilde{\tilde{L}}_4 = \tilde{L}_4, \qquad \tilde{\tilde{L}}_5 = \left(\tilde{L}_5 + \frac{c_d c_m}{M_S^2}\right) = \frac{F_0^2}{4M_S^2}, \quad (32)$$

where we considered the large–N_C high-energy constraints $\tilde{L}_4 = \tilde{L}_5 = 0$ and $(4c_d c_m/F_0^2) = 1$ from the scalar form factor [44]. At LO in $1/N_C$ this yields the prediction [9]

$$F_\phi = F_0\left(1 + \frac{4c_d c_m}{F_0^2}\frac{m_\phi^2}{M_S^2}\right) = F_0\left(1 + \frac{m_\phi^2}{M_S^2}\right), \quad (33)$$

which reproduce the F_π and F_K lattice data fairly well up to pion masses of the order of 700 MeV [9]. The large–N_C relation $c_d = c_m$ [44] was used in Ref. [9] to produce Eq. (33), where it led to the relation $m_\phi^2 = B_0(m_{q_1} + m_{q_2})$ between the pNGB mass and the masses of its two valence quarks. We have also used that $\tilde{F}/F_0 = 1$ and $\Sigma_{\phi.1\ell} = F_{\phi,1\ell}^{1\mathrm{PI}} = 0$ when $N_C \to \infty$. The only region where this description deviated significantly from the data was in the light pion mass range, where the chiral logs need to be included to properly reproduce the lattice simulation in that regime [15,16]. Here in Eq. (33) the coupling F_0 implicitly refers to the $n_f = 3$ decay constant in that same limit, this is, at large N_C.

In summary, our calculation of the pNGB decay constants F_ϕ (with $\phi = \pi, K$) is sorted out in the form

$$\frac{F_\phi}{F_0} = \left.\frac{\Delta F_\phi}{F_0}\right|_{\mathcal{O}(N_C^0)} + \left.\frac{\Delta F_\phi}{F_0}\right|_{\mathcal{O}(N_C^{-1})} + \ldots\ldots \quad (34)$$

with the dots standing for terms of $\mathcal{O}(N_C^{-2})$ and higher, which will be neglected in the present article. In the joined large–N_C and chiral limits one has the right-hand side become equal to one by construction, as $F_0 = \lim_{m_{u,d,s}\to 0} F_\phi$. At large–$N_C$, the relevant couplings in the quark mass corrections to F_ϕ are related to the scalar form factor and can be fixed through high-energy constraints [9,44]. However, one should be aware that it is not possible to have a full control of the quark mass corrections beyond the linear m_q term. In fact, including all possible m_q^2 corrections corresponds to considering the full sets of local $\mathcal{O}(p^6)$ operators without resonance fields. The complexity of higher order m_q corrections not only happens for the NLO in N_C but also for the LO case. For instance, large–N_C contributions to the scalar (vector) multiplet

mass splitting can be in principle of an arbitrary order in m_q, leading to LO (NLO) corrections in $1/N_C$ to F_ϕ with arbitrary powers of the quark mass. Clearly, there is not a uniquely defined truncation procedure.

B. Renormalization in RχT

The calculation of the Feynman diagrams contributing to F_ϕ up to NLO in $1/N_C$ is straightforward (Figs. 2 and 3), though the final results are quite lengthy and have been relegated to Appendix C for the sake of clarity and in order not to interrupt our discussion. We take into account the m_q dependence of the resonance masses in the propagators in the loops, which is given by Eq. (19).

In order to have finite results for the physical quantities F_π and F_K, the next step consists of performing the renormalization. As in conventional χPT [4] we use the dimensional regularization method and the $\overline{\text{MS}}-1$ renormalization scheme where we will subtract from the Feynman integrals the UV divergence

$$\frac{1}{\hat{\epsilon}} = \mu^{-2\epsilon}\left(\frac{1}{\epsilon} - \gamma_E + \ln 4\pi + 1\right) = \frac{1}{\epsilon} - \gamma_E + \ln 4\pi + 1 - \ln\mu^2 + \mathcal{O}(\epsilon), \qquad \left(\epsilon = 2 - \frac{D}{2}\right). \tag{35}$$

The UV divergences from loops can be absorbed through a convenient renormalization of the RχT couplings $C_\chi = \tilde{F}, \tilde{\tilde{L}}_4, \tilde{\tilde{L}}_5$ in the form

$$C_\chi = C_\chi^r(\mu) + \delta C_\chi(\mu), \tag{36}$$

where the $C_\chi^r(\mu)$ are the finite renormalized couplings and the counterterms $\delta C_\chi(\mu)$ are infinite and cancel out the one-loop UV divergences. The $\overline{\text{MS}}-1$ scheme is usually employed in χPT and RχT, where the subtracted divergence is of the form

$$\delta C_\chi(\mu) = -\frac{\Gamma^{C_\chi}}{32\pi^2}\frac{1}{\hat{\epsilon}}, \tag{37}$$

and the renormalized coupling has a renormalization group running given by

$$\frac{dC_\chi(\mu)}{d\ln\mu^2} = -\frac{\Gamma^{C_\chi}}{32\pi^2}. \tag{38}$$

This will be the scheme considered to renormalize $\tilde{\tilde{L}}_4$ and $\tilde{\tilde{L}}_5$ in this article. More precisely, the renormalization of $\tilde{\tilde{L}}_4 = \tilde{L}_4$ and $\tilde{\tilde{L}}_5 = \tilde{L}_5 + c_d c_m/M_S^2$ is given by

$$\Gamma^{\tilde{\tilde{L}}_4} = \frac{1}{8}\left[1 + \frac{4c_d c_m}{F_0^2} + \frac{2c_d^2}{F_0^2}(1-4e_m^S) - \frac{3G_V^2}{F_0^2}(1-4e_m^V)\right],$$
$$\Gamma^{\tilde{\tilde{L}}_5} = \frac{3}{8}\left[1 - \frac{4c_d c_m}{F_0^2} + \frac{2c_d^2}{F_0^2}(1-4e_m^S) - \frac{3G_V^2}{F_0^2}(1-4e_m^V)\right]. \tag{39}$$

One may compare this result with that in $SU(3)$ χPT, $\Gamma^{L_5^{\chi\text{PT}}} = 3\Gamma^{L_4^{\chi\text{PT}}} = 3/8$ [4].

The $\overline{\text{MS}}-1$ one-loop renormalization $\delta\tilde{F}$ is found to be

$$\frac{\delta\tilde{F}}{F_0} = -\frac{1}{16\pi^2}\left(\frac{3c_d^2M_S^2}{F_0^4} + \frac{2c_d^2M_0^2}{3F_0^4} - \frac{9G_V^2M_V^2}{2F_0^4}\right)\frac{1}{\hat{\epsilon}}. \tag{40}$$

This result recovers the scalar and vector resonance contributions obtained in Ref. [10]. Though the M_0 term in the previous equation is in principle $1/N_C$ suppressed, it can be important in the phenomenological discussion as its numerical value of M_0 is not small. Due to the inclusion of the heavier resonance states and the singlet η_1, the renormalization in RχT is a bit different from the conventional one in χPT with only pNGB. Indeed, it resembles a bit the situation in Baryon χPT, where the loops generate power-counting breaking terms which contribute at all orders in the chiral expansion [45]. For instance, based on dimensional analysis [3] one can prove that the $\mathcal{O}(p^2)$ coupling F_0 does not get renormalized at any order in χPT since any possible loop correction is always $\mathcal{O}(p^4)$ or higher. This is not the case in RχT, where in general one needs to renormalize the couplings of the LO Lagrangian to cancel out the one-loop UV divergences [10,13,37]. Moreover, though subleading in $1/N_C$, the RχT loops with massive states generate power-counting breaking terms from the point of view of the χPT chiral counting, in the same way as it happens in baryon χPT [45]. We will explicitly see in the next section that, the matching of the RχT and χPT results in the low-energy region fixes completely the LO coupling $\tilde{F}$ and solve the problem with the power-counting breaking terms.

Notice that in the present work, after the renormalizations of $\tilde{F}, \tilde{\tilde{L}}_4$, and $\tilde{\tilde{L}}_5$, we obtain a finite result for our physical observables F_π and F_K. In other words, all the one-loop UV divergences of the pion and kaon decay constant calculation can be canceled out through the convenient renormalizations $\delta\tilde{F}, \delta\tilde{\tilde{L}}_4$, and $\delta\tilde{\tilde{L}}_5$.

C. Matching RχT and χPT

In order to establish the relation between the χPT LECs and the couplings from RχT, it is necessary to perform the chiral expansion of the decay constants calculated in RχT and then match with the pure χPT results. This procedure resembles the reabsorption of the power breaking terms into the lower order couplings in baryon χPT [45]. In such a

way, we can relate the χPT LECs with the resonance couplings including not only the leading order contributions in $1/N_C$ but also the $1/N_C$ corrections.

The pNGB decay constants are given in $SU(3)$ χPT up to $\mathcal{O}(p^4)$ by Ref. [4]

$$F_\pi = F_0\left(1+\frac{4L_4^{\chi\mathrm{PT}}(2m_K^2+m_\pi^2)}{F_0^2}+\frac{4L_5^{\chi\mathrm{PT}}m_\pi^2}{F_0^2} -\frac{1}{2F_0^2}[2iA_0(m_\pi^2)+iA_0(m_K^2)]\right),$$
$$F_K = F_0\left(1+\frac{4L_4^{\chi\mathrm{PT}}(2m_K^2+m_\pi^2)}{F_0^2}+\frac{4L_5^{\chi\mathrm{PT}}m_K^2}{F_0^2} -\frac{3}{8F_0^2}[iA_0(m_\pi^2)+2iA_0(m_K^2)+iA_0(m_{\eta_8}^2)]\right), \quad (41)$$

with $m_{\eta_8}^2=(4m_K^2-m_\pi^2)/3$ and the one-point Feynman integral $A_0(m^2)$ is given in Appendix A whose UV divergences are conveniently renormalized through $L_4^{\chi\mathrm{PT}}$ and $L_5^{\chi\mathrm{PT}}$.

The chiral singlet pNGB η_1 requires a particular treatment. When the chiral expansion of the RχT expressions is performed to match $SU(3)$–χPT, we do not take the singlet η_1 mass M_0 as a small expansion parameter. Instead, we keep its full contribution in spite of its effect being suppressed by $1/N_C$. It is known that in the low-energy EFT where the η' has been integrated these contributions may become phenomenologically important [26]. Expanding the decay constants in RχT in powers of m_ϕ^2 and then matching with $SU(3)$–χPT up to $\mathcal{O}(p^4)$, we obtain the following relations

$$1=\frac{\tilde{F}^r(\mu)}{F_0}+\frac{1}{16\pi^2}\left[\frac{c_d^2M_S^2}{F_0^4}\left(\frac{7}{6}-\frac{7}{3}\ln\frac{M_S^2}{\mu^2}\right)+\frac{c_d^2}{3F_0^4}\frac{M_S^4-M_0^4+2M_0^4\ln\frac{M_0^2}{\mu^2}-2M_S^4\ln\frac{M_S^2}{\mu^2}}{M_S^2-M_0^2}+\frac{G_V^2M_V^2}{F_0^4}\left(\frac{3}{4}+\frac{9}{2}\ln\frac{M_V^2}{\mu^2}\right)\right], \quad (42)$$

$$L_4^{\chi\mathrm{PT},r}(\mu)=\tilde{\tilde{L}}_4^{\,r}(\mu)+\frac{1}{16\pi^2F_0^2}\left\{\frac{c_d^2}{144(M_S^2-M_0^2)^2}\left[(M_0^2-9M_S^2)(M_0^2-M_S^2)+8M_0^4\ln\frac{M_0^2}{\mu^2}-2(13M_0^4-18M_0^2M_S^2+9M_S^4)\ln\frac{M_S^2}{\mu^2}\right]\right.$$
$$\left.+\frac{1}{8}c_dc_m-\frac{1}{4}c_dc_m\ln\frac{M_S^2}{\mu^2}+\frac{1}{32}G_V^2+\frac{3}{16}G_V^2\ln\frac{M_V^2}{\mu^2}+c_d^2e_m^S\left(\frac{1}{4}+\frac{1}{2}\ln\frac{M_S^2}{\mu^2}\right)-G_V^2e_m^V\left(\frac{7}{8}+\frac{3}{4}\ln\frac{M_V^2}{\mu^2}\right)\right\}, \quad (43)$$

$$L_5^{\chi\mathrm{PT},r}(\mu)=\tilde{\tilde{L}}_5^{\,r}(\mu)+\frac{1}{16\pi^2F_0^2}\left\{\frac{c_d^2}{48(M_0^2-M_S^2)}\left[9(M_0^2-M_S^2)-16M_0^2\ln\frac{M_0^2}{\mu^2}-2(M_0^2-9M_S^2)\ln\frac{M_S^2}{\mu^2}\right]\right.$$
$$+\frac{c_d^2e_m^S}{12(M_S^2-M_0^2)^2}\left[(M_0^2-9M_S^2)(M_0^2-M_S^2)+8M_0^4\ln\frac{M_0^2}{\mu^2}+2(5M_0^4-18M_0^2M_S^2+9M_S^4)\ln\frac{M_S^2}{\mu^2}\right]$$
$$\left.-\frac{3}{8}c_dc_m+\frac{3}{4}c_dc_m\ln\frac{M_S^2}{\mu^2}+\frac{3}{32}G_V^2+\frac{9}{16}G_V^2\ln\frac{M_V^2}{\mu^2}-G_V^2e_m^V\left(\frac{21}{8}+\frac{9}{4}\ln\frac{M_V^2}{\mu^2}\right)\right\}. \quad (44)$$

We have matched the chiral expansion of our RχT predictions for F_ϕ in powers of the quark masses m_q [on the right-hand side of Eqs. (42)–(44)] to the corresponding chiral expansion in χPT [left-hand side of Eqs. (42)–(44)]. Equation (42) stems from the matching at $\mathcal{O}(m_q^0)$ and Eqs. (43) and (44) are derived from the chiral expansion at $\mathcal{O}(m_q^1)$. The one-loop contributions in Eq. (41) are exactly matched and one recovers the correct running for the $L_4^{\chi\mathrm{PT}}(\mu)$ and $L_5^{\chi\mathrm{PT}}(\mu)$ predictions. Notice that if we took the on-shell renormalization scheme from Ref. [10] instead of the $\overline{\mathrm{MS}}-1$ scheme considered here Eq. (42) would become $1=\tilde{F}^r/F_0$.

The final renormalized expression for the pNGB decay constants is

$$F_\phi = F_0\left[1+\frac{4\tilde{\tilde{L}}_4^{\,r}(2m_K^2+m_\pi^2)}{F_0^2}+\frac{4\tilde{\tilde{L}}_5^{\,r}m_\phi^2}{F_0^2}+\frac{F_{\phi,1\ell}^{1\mathrm{PI,r}}}{F_0} +\frac{1}{2}\Sigma'^r_{\phi,1\ell}+\left(\frac{\tilde{F}^r}{F_0}-1\right)\right], \quad (45)$$

with the last term $(\frac{\tilde{F}^r}{F_0}-1)$ given by the matching condition in Eq. (42). This ensures that the renormalized contributions from the one-loop diagrams are appropriately canceled out in the chiral limit so that the decay constants F_ϕ become equal to F_0 when $m_q\to 0$. In the same way, in our later analysis, $\tilde{\tilde{L}}_4^{\,r}$ and $\tilde{\tilde{L}}_5^{\,r}$ will be expressed in terms of $L_4^{\chi\mathrm{PT},r}$ and $L_5^{\chi\mathrm{PT},r}$, respectively, by means of the χPT

matching relations in Eqs. (43) and (44). This will allow us to deal in a more direct and convenient way with the χPT LECs in our RχT predictions. Our theoretical predictions for F_ϕ will depend only on

Tree-level contributions:

$$\tilde{F}^r\{\to F_0\}, \qquad \tilde{\tilde{L}}_4^r\{\to L_4^{\chi\mathrm{PT},r}\}, \qquad \tilde{\tilde{L}}_5^r\{\to L_5^{\chi\mathrm{PT},r}\}, \tag{46}$$

$$\textbf{One-loop contributions}: e_m^V, \quad e_m^S, \quad c_m, \quad c_d, \quad G_V, \quad M_V, \quad M_S, \quad M_0. \tag{47}$$

The tree-level contributions from $\tilde{F}$, $\tilde{\tilde{L}}_4^r(\mu)$ and $\tilde{\tilde{L}}_5^r(\mu)$ will be expressed in terms of F_0, $L_4^{\chi\mathrm{PT},r}(\mu), L_5^{\chi\mathrm{PT},r}(\mu)$ in the phenomenological analysis. As we are carrying our decay constant computation up to NLO in $1/N_C$, the LECs of F_0, $L_4^{\chi\mathrm{PT},r}(\mu), L_5^{\chi\mathrm{PT},r}(\mu)$ correspond to the renormalized couplings at that order, not just their large–N_C values. In contrast, the remaining parameters only appear within loops. They do not get renormalized at this order and correspond to their large–N_C values. In our fits to lattice simulations we will always fit the parameters in the first line of Eq. (47), we will use high-energy constraints for those in the second line (although we will also check the impact of fitting G_V or setting it to particular values), and the parameters in the third line of Eq. (47) will be always introduced as inputs.

We will also analyze the lattice results for the ratio F_K/F_π. Following the principle considered before, we will fit the data with our theoretical prediction expanded up to NLO:

$$\frac{F_K}{F_\pi} = 1 + \frac{4\tilde{\tilde{L}}_5^r(m_K^2 - m_\pi^2)}{F_0^2} + \left(\frac{F_{K,1\ell}^{1\mathrm{PI,r}}}{F_0} + \frac{1}{2}\Sigma'^r_{K,1\ell}\right) - \left(\frac{F_{\pi,1\ell}^{1\mathrm{PI,r}}}{F_0} + \frac{1}{2}\Sigma'^r_{\pi,1\ell}\right). \tag{48}$$

Apart from the present analysis of lattice data, Eqs. (43) and (44) also can be employed to predict the $L_4^{\chi\mathrm{PT}}$ and $L_5^{\chi\mathrm{PT}}$ chiral LECs in terms of resonance parameters. These NLO expressions fully recover the one-loop running of the LECs and can be used to extract the chiral couplings at any renormalization scale μ. Furthermore, by imposing high-energy constraints in the way previously considered in analogous one-loop analyses [10–12], it should be possible to provide similar NLO predictions in $1/N_C$ in terms of F_0 and the resonance masses M_R.

IV. PHENOMENOLOGICAL DISCUSSIONS

A. Inputs and constraints

As previously mentioned in the Introduction, we confront our theoretical calculation of the pNGB decay constants to the lattice data from different lattice collaborations [15–19].

In addition, we also take into account the lattice determination of the $\rho(770)$ mass with varying quark masses [46–49], which helps us to constrain the vector mass splitting coupling e_m^V in Eq. (18). For the scalar resonances, as we mentioned previously, we only consider those that survive at large N_C. In fact, this is not a settled problem yet. For example, the inverse amplitude method analyses [28] found that the $f_0(500)$ or σ resonance could fall down to the real axis at large values of N_C, meaning that it survives as a conventional $\bar{q}q$ state at large N_C, while the $f_0(980)$ disappears in that limit. In the N/D approach, the situation is just the opposite [29–31]. However it is interesting to point out that though the resonance trajectories for $N_C = 3$ to ∞ are quite different in the two approaches, there is an important common conclusion: a scalar resonance with mass around 1 GeV at large N_C is necessary to fulfill the semilocal duality in $\pi\pi$ scattering. In Refs. [29–31], it was also proved that the 1 GeV scalar resonance at large N_C is needed to satisfy the Weinberg sum rules in the scalar and pseudoscalar sectors. Therefore it seems proper to set the bare scalar resonance mass at large N_C around 1 GeV. This is also supported by our previous analysis in Ref. [27]. In the following we take the result $M_S = 980$ GeV from Ref. [27] as an input while the value of the scalar mass splitting coupling e_m^S will be fitted in this work, as the value in the previous reference is determined with too large error bars.

The leading order expressions have been employed in our theoretical analysis to relate the squared kaon mass with the varying squared pion mass and $m_{u/d}$:

$$m_\pi^2 = 2Bm_{u/d}, \tag{49}$$

$$m_K^2 = B(m_s + m_{u/d}) = \left(m_{K,\mathrm{phys}}^2 - \frac{m_{\pi,\mathrm{phys}}^2}{2}\right)\alpha_{m_s} + \frac{m_\pi^2}{2}, \tag{50}$$

where $m_{K,\mathrm{phys}}$ and $m_{\pi,\mathrm{phys}}$ denote the physical masses of kaon and pion. Different values of $\alpha_{m_s} = m_s/m_{s,\mathrm{phys}}$ correspond in this equation to the situations with different strange quark masses whereas $\alpha_{m_s} = 1$ refers to the physical m_s case. We will always take $\alpha_{m_s} = 1$ in all the fits in this article, considering only lattice simulation data with $m_s = m_{s,\mathrm{phys}}$. Later on, after performing the fit, we will study to what extent our results depend on the linear quark mass relations in Eqs. (49) and (50) by varying α_{m_s}. Indeed, this insensitivity to higher order corrections was already observed for $m_\pi^2/(2Bm_{u/d})$ [19,50]. This ratio was

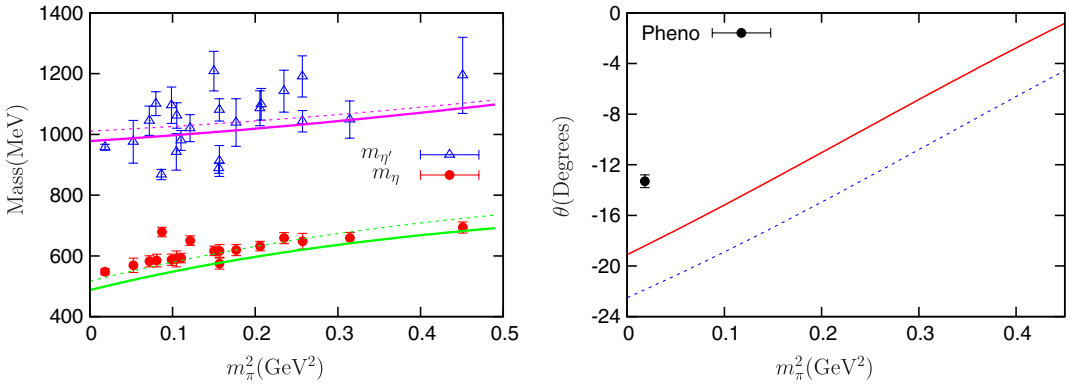

FIG. 4 (color online). Masses and mixing angle of η and η'. The points in the left panel are taken from Ref. [51], which summarizes the data from ETM [52], RBC-UKQCD [53], HSC [54], and UKQCD [55] collaborations. The mixing angle $\theta = (-13.3 \pm 0.5)^\circ$ extracted in the phenomenological analysis [35] for physical masses is plotted in the right panel. The solid lines are obtained by using the physical strange quark mass ($m_s = m_{s,\mathrm{Phys}}$) and the dashed lines come from employing $m_s = 1.2 m_{s,\mathrm{Phys}}$. The value $M_0 = 850$ MeV is taken as input [25]. We remind the reader this plot is a prediction, not a fit.

found to show a very small dependence on $m_{u/d}$ in the whole range of values of the simulation [19,50], supporting the description given by Eqs. (49) and (50) and used in this article.

Since the η and η' only enter the expressions of F_π and F_K through the chiral loops, it is enough to consider the leading order mixing produced by the Lagrangian (13) for their masses and mixing angle (see Appendix B for details). The chiral limit of the singlet η_1 mass (M_0) is by definition independent of the light quark mass and will take the fixed value $M_0 = 850$ MeV in this article [25]. In Fig. 4 one can see the fair agreement of the LO prediction with lattice simulations [51–55] and previous phenomenological analyses [35] for the physical quark mass. The one-parameter fit to lattice data [51–55] for m_η and $m_{\eta'}$ (Fig. 4) yields essentially the same value ($M_0 \simeq 835$ MeV), very close to the input $M_0 = 850$ MeV which will be employed all through the paper and indistinguishable in Fig. 4 when plotted.

In Fig. 4, the solid lines correspond to our predictions with $\alpha_{m_s} = 1$ and the dashed lines refer to the case with $\alpha_{m_s} = 1.2$. It is clear that the change caused by using different strange quark masses in $\eta - \eta'$ mixing is mild. On the other hand, it is remarkable that the leading order mixing from $U(3) - \chi$PT can reasonably reproduce the lattice simulation data for the masses of η and η', as shown in the left panel of Fig. 4. In the right panel, we show the leading order mixing angle θ with varying pion masses, i.e., with varying light u/d quark masses. As expected, when the u/d quark mass approaches to the strange quark mass, i.e., the pion mass tends to the kaon mass, there is no mixing between η_1 and η_8, as their mixing strength is proportional to the $SU(3)$ breaking $m_K^2 - m_\pi^2$. Likewise, this result gives extra support to the linear dependence on the light quark masses for m_ϕ^2 assumed in Eqs. (49) and (50) as an approximation in this article.

In the fit, we will use the chiral limit mass of the vector resonance multiplet computed in Ref. [27] as an input:

$$M_V = 764.3 \text{ MeV}. \tag{51}$$

Imposing the high energy constraints dictated by QCD is an efficient way to reduce the free couplings in effective field theory. In addition it makes the effective field theory inherit more properties from QCD. In RχT literature, it is indeed quite popular to constrain the resonance couplings through the high energy behaviors of form factors [12,44], meson-meson scattering [29,56], Green functions [10], tau decay form-factors [57,58], etc. Among the various constraints obtained in literature, two of them are relevant to our current work

$$c_d = \frac{F_0^2}{4c_m}, \tag{52}$$

$$G_V = \sqrt{\frac{F_0^2 - 2c_d^2}{3}}, \tag{53}$$

resulting from the analyses of the scalar form factor [44] and partial-wave $\pi\pi$ scattering [56] at large N_C, respectively.

The renormalization scale μ will be set at 770 MeV, corresponding the renormalized LECs determined later to their values at that scale.

B. Fit to lattice data

We use the CERN MINUIT package to perform the fit. The values of the six free parameters from the fit read

$$F_0 = 80.0 \pm 1.0 \text{ MeV}, \quad L_4^{\chi\mathrm{PT}} = (-0.11 \pm 0.06) \times 10^{-3},$$
$$L_5^{\chi\mathrm{PT}} = (0.59 \pm 0.08) \times 10^{-3}, \quad c_m = 54.5 \pm 3.3 \text{ MeV},$$
$$e_m^V = -0.236 \pm 0.005, \quad e_m^S = -0.204 \pm 0.024, \tag{54}$$

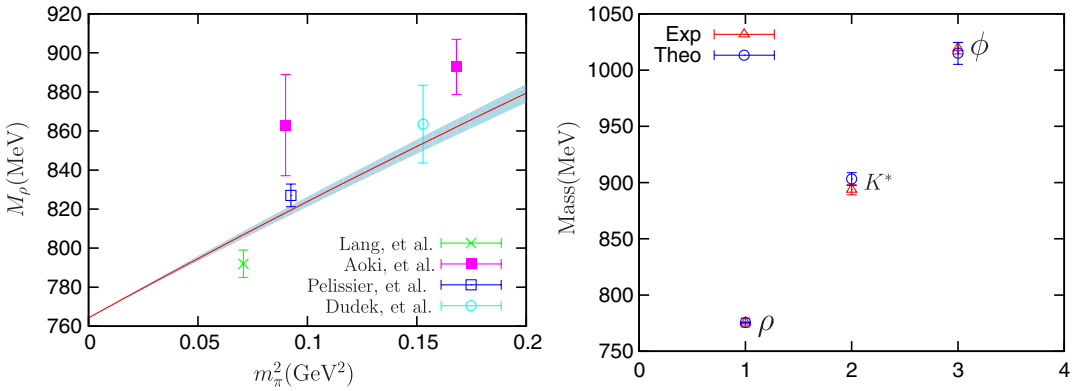

FIG. 5 (color online). Fit results for the vector masses. The left panel shows the square pion mass dependence of M_ρ. The lattice data in this panel are taken from Refs. [46–49]. The right panel shows the masses of $\rho(770)$, $K^*(892)$, and $\phi(1020)$ with the physical pion mass. The shaded area in the left panel and the empty circles in the right panel represent our estimation of the error bands, which are explained in detail in the text.

with $\chi^2/\text{d.o.f} = 90.8/(52-6)$. The strange quark mass is kept fixed to $m_{s,\text{phys}}$ in this fit. We point out that one should take the value of χ^2 from the fit as a mere orientation of the goodness of the fit rather than in its precise statistical sense: lattice simulation results should not be taken as real experimental data for various quark masses as they are in general highly correlated and systematic uncertainties should be also properly accounted. This gets even worse when combining data from different groups. For a detailed discussion see Ref. [19]. The aim of this work is to provide a first quantitative analysis of the potentiality of these types of hadronic observables, i.e., F_π and F_K, for the study of resonance properties.

By substituting the results from Eq. (54) in the high energy constraints given in Eqs. (52) and (53) one gets

$$c_d = 29.3 \pm 1.9 \text{ MeV}, \qquad G_V = 39.5 \pm 0.9 \text{ MeV}. \quad (55)$$

The negative values for e_m^R indicate that the resonance masses grow with m_q as one can see from Eq. (19). They are found in agreement with the previous estimates $e_m^V = -0.228 \pm 0.015$ and $e_m^S = -0.1 \pm 0.9$ [27]. The present determinations for c_d and c_m are compatible with those in Ref. [27]: $c_d = 26 \pm 7$ MeV and $c_m = 80 \pm 21$ MeV. Nonetheless, we find large discrepancies for the value of the $\rho - \pi\pi$ coupling given in Ref. [27]: $G_V = 63.9 \pm 0.6$ MeV. The reason for the large discrepancies of the G_V values will be analyzed in detail in next section.

In the left panel of Fig. 5, we show our fit results together with the lattice data for M_ρ with different pion masses, which are originally taken from Refs. [46–49]. Due to the large error bars of these data, the stringent constraint on the vector mass splitting parameter e_m^V comes from the determination of physical masses of ρ, K^*, and ϕ, which are shown in the right panel of Fig. 5. This explains in part the very similar results between our current value for e_m^V and that in Ref. [27].

The light-blue and criss-cross shaded areas surrounding the solid lines in Figs. 5 and 6 represent our estimates of the 68% confidence level (CL) error bands. In order to obtain these uncertainty regions we first generate large sets of parameter configurations by varying all our 6 fit parameters around their central values randomly via a Monte Carlo (MC) generator; then we use these large amounts of parameter configurations to calculate the χ^2 and keep only the configurations with χ^2 smaller than $\chi_0^2 + \Delta\chi^2$, being χ_0^2 the minimum chi-square obtained from the fit. The 68% CL region is given by $\Delta\chi^2 = 7.04$ for a 6–parameter fit. [3] The successful parameter configurations provide the 68% CL error bands. In such a way, the correlations between the different fit parameters in Eq. (54) have been taken into account when plotting the error bands in Figs. 5 and 6.

Both our fit results and the lattice simulation data for F_π and F_K with varying pion masses are shown in the left panel of Fig. 6. The lattice data for F_π and F_K are taken from MILC [15,16], RBC, and UKQCD [17,18]. Concerning the data from Refs. [17,18], we only consider those that are simulated with the physical strange quark mass and the unitary points. In the right panel, we give the plots for the ratio F_K/F_π [19]. Even though the fit is performed with $m_s = m_{s,\text{phys}}$, we have also plotted in Fig. 6 the predictions for F_π and F_K with $m_s = 1.2 m_{s,\text{phys}}$. For this we have used the fit values from Eq. (54). In the left panel of Fig. 6, one can see how the results with physical strange quark mass (solid lines) vary when one instead uses $\alpha_{m_s} = 1.2$ in Eq. (50) (dashed lines). In the right panel of Fig. 6, the solid red line (lower) corresponds to the fit result with the perturbative expansion of F_K/F_π up to one loop

[3]The number $\Delta\chi^2 = 7.04$ is obtained from the standard multivariable Gaussian distribution analysis for a 68% CL region in a 6–parameter fit [59]. For a general $(1-\alpha)$ CL and number of parameters m, $\Delta\chi^2$ is given by $\alpha = \Gamma(\frac{m}{2}, \frac{\Delta\chi^2}{2})/\Gamma(\frac{m}{2})$, with $\Gamma(b,x)$ and $\Gamma(b)$ the incomplete gamma and Euler gamma functions, respectively.

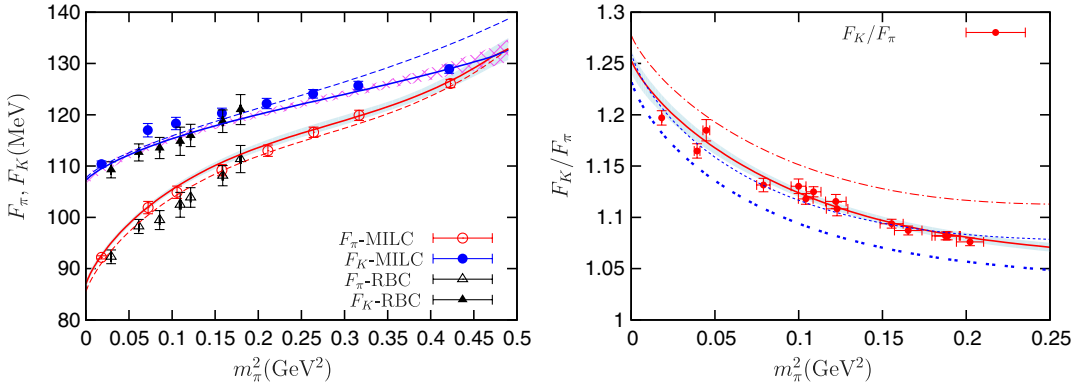

FIG. 6 (color online). Fit results for F_π, F_K, together with the lattice data from MILC [15,16], RBC, and UKQCD [17,18] collaborations are shown in the left panel. The light blue and criss-cross band provide the 68% CL regions in both plots. In the right panel, we plot the ratio F_K/F_π together with the lattice data from Ref. [19]. The leftmost data points in each panel correspond to the physical mass values, which are taken from PDG [59]. The solid lines in the left panel are the fit results with physical strange quark mass. The solid red (lower) and double-dashed blue (lower) lines in the right-hand plot refer to the expanded [Eq. (48)] and unexpanded [Eq. (45)] expressions for F_K/F_π with $\alpha_{m_s} = 1$, respectively. The dashed lines in the left panel correspond to $\alpha_{m_s} = 1.2$. The same applies to the dash-dotted red (upper) and dashed blue (upper) lines in the right-hand plot, which refer to the expanded [Eq. (48)] and unexpanded [Eq. (45)] expressions for F_K/F_π, respectively.

order in Eq. (48) with $m_s = m_{s,\text{phys}}$, whereas the dash-dotted red (upper) line uses Eq. (48) with $m_s = 1.2m_{s,\text{phys}}$. The blue double-dashed (lower) line represents the unexpanded value of F_K/F_π extracted directly from F_π and F_K from Eq. (45) with $m_s = m_{s,\text{phys}}$, while the blue dashed (upper) line uses the same unexpanded expression but with $m_s = 1.2m_{s,\text{phys}}$.

Using a value of the strange quark mass 20% larger than the physical one only induces slight changes for F_π and F_K in the region of $m_\pi \leq 500$ MeV, indicating the smaller sensitivity of these two quantities to the linear quark mass dependence for m_ϕ^2 assumed in Eqs. (49) and (50). Notice that F_π decreases when m_s increases, while F_K grows. The reason is the different way how m_s enters in these two observables: through loops and $1/N_C$ suppressed in F_π and in the valence quarks and contributing at LO in $1/N_C$ for F_K. This explains the larger shift observed in the F_K/F_π ratio when varying the strange quark mass (see the right panel in Fig. 6).

C. Anatomy of the fit parameters: Correlations

For the scalar resonance parameters c_d and c_m, our current results are quite compatible with those determined in many other processes [7,27,29,31,44,60]. However, the present determination of G_V in Eq. (55) is clearly lower than the usual results from phenomenological analyses, which prefer values around 60 MeV [7,27,29,31]. One way out of this problem is to free G_V in our fit, instead of imposing its large–N_C high energy constraint from Eq. (53).

A first test is provided by setting G_V to particular values. In Fig. 7, we plot the 68% CL regions for $L_4^{\chi\text{PT}}$ and $L_5^{\chi\text{PT}}$ for the fits with G_V fixed to $G_V = 40, 50, 60, 70$ MeV (ellipses from top-right to bottom-left in Fig. 7, respectively; Gaussianity is assumed). This shows how the $\rho - \pi\pi$ coupling affects the determinations of $L_4^{\chi\text{PT}}$ and $L_5^{\chi\text{PT}}$: smaller values of G_V lead to a closer agreement with the standard χPT phenomenology [4,5]. On the other hand, larger values of G_V tend to decrease the values of both LECs; eventually, for a large enough $\rho - \pi\pi$ coupling, $L_5^{\chi\text{PT}}$ turns negative and $L_4^{\chi\text{PT}}$ violates the paramagnetic inequality $F^{n_f=3} < F^{n_f=2}$ ($L_4^{\chi\text{PT}}(\mu) > -0.4 \times 10^{-3}$ for $\mu = 770$ MeV [22,61]). This effect cannot be attributed to an inappropriate description of the kaon and pion masses in Eqs. (49) and (50) nor the fact of neglecting operators of the Lagrangian whose contributions to F_ϕ are suppressed by both $1/N_C$ and m_ϕ^4/M_S^4. This can be neatly observed in Fig. 7, where the black ellipses are given by the fit to the full set of lattice data whereas only the data with $m_\pi < 500$ MeV are used in the fits that provide the light-green regions. Reducing the number of data points in the large pion mass region obviously leads to a consistent enlargement of the uncertainty regions but does not modify at all the strong correlation with G_V.

A second test consists on exploring two alternative versions of the high energy constraints for the $\rho - \pi\pi$ coupling in Eq. (53): $G_V = F_0/\sqrt{2}$ [64] and $G_V = F_0/\sqrt{3}$ [29,56]. The former constraint corresponds to the original Kawarabayashi-Suzuki-Riazuddin-Fayyazuddin (KSRF) relation while the latter is the extended KSRF relation obtained by including the crossed-channel contributions and ignoring the scalar resonances in $\pi\pi$ scattering. We obtain $G_V \sim 58$ MeV for $G_V = F_0/\sqrt{2}$ and $G_V \sim 47$ MeV for $G_V = F_0/\sqrt{3}$, with the chiral coupling F_0 remaining always stable and with a value around 82 MeV. In both

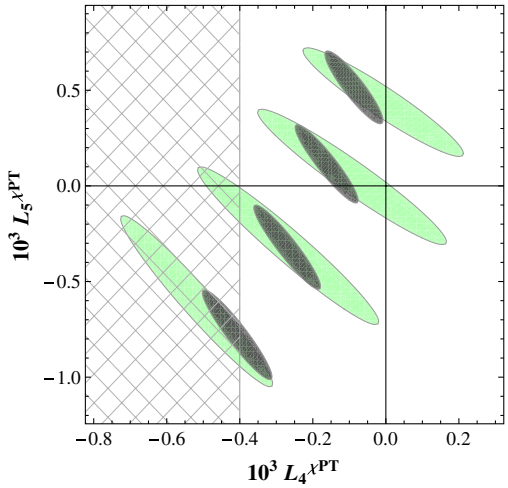

FIG. 7 (color online). 68% CL regions for $L_4^{\chi\mathrm{PT}}(\mu)$ and $L_5^{\chi\mathrm{PT}}(\mu)$ at $\mu = 770$ MeV for the fits with G_V fixed to 40, 50, 60, and 70 MeV (respectively from top-right to bottom-left). Here and in the following plots the criss-cross area (left-hand side of this figure) represents the region forbidden by the paramagnetic inequality $F^{n_f=3} < F^{n_f=2}$, which implies $L_4^{\chi\mathrm{PT}}(\mu) > -0.4 \times 10^{-3}$ for $\mu = 770$ MeV [22,61]. The light-green ellipses come from fits to data points with $m_\pi < 500$ MeV and the darker gray ones from the fits to all data.

situations, we confirm the findings we obtained previously when G_V was fixed at the specific values 40, 50, 60, and 70 MeV (see Fig. 7): we observe strong anticorrelations between $L_4^{\chi\mathrm{PT}}$ and $L_5^{\chi\mathrm{PT}}$ and their values are strongly affected by G_V in the way discussed before. The values of $L_4^{\chi\mathrm{PT}}$ and $L_5^{\chi\mathrm{PT}}$ follow closely the trend shown in Fig. 7: the smaller G_V becomes, the more negative $L_4^{\chi\mathrm{PT}}$ and $L_5^{\chi\mathrm{PT}}$ turn. Hence we conclude that our second test based on using different high energy constraints for G_V confirms our former findings and does not reveal new information with respect to the first test, where G_V was fixed at specific values.

We will proceed now with our third test: G_V will be set free and fitted together with the other six parameter from the previous analysis. Statistically speaking, we do not find any significant improvement of the fit quality by releasing this additional free parameter, but we do see obvious changes with respect to the values in Eq. (54), which now turn out to be

$$\begin{aligned} &F_0 = 83.5 \pm 1.5\ \mathrm{MeV}, \quad L_4^{\chi\mathrm{PT}} = (-0.31 \pm 0.10) \times 10^{-3}, \\ &L_5^{\chi\mathrm{PT}} = (-0.46 \pm 0.33) \times 10^{-3}, \quad c_m = 64.1 \pm 3.7\ \mathrm{MeV}, \\ &e_m^V = -0.236 \pm 0.004, \quad e_m^S = -0.540 \pm 0.088, \\ &G_V = 63.0 \pm 6.4\ \mathrm{MeV}, \end{aligned} \tag{56}$$

with $\chi^2/(\mathrm{d.o.f}) = 80.0/(52-7)$. The fit quality resulting in this case is quite similar to that in the previous section. By substituting the results from Eq. (56) in the scalar form-factor high energy constraints from Eq. (52) one obtains

$$c_d = (27.2 \pm 1.8)\ \mathrm{MeV}. \tag{57}$$

The most striking change happens for $L_5^{\chi\mathrm{PT}}$, whose sign becomes negative. However, according to most phenomenological determinations of $L_5^{\chi\mathrm{PT}}$ in literature [5,22,62] its value must be positive. Also RχT predicts a positive $L_5^{\chi\mathrm{PT}}$ at large N_C [7]. Hence the resulting parameters in Eq. (56) do not seem to correspond to the physical solution. The reason behind this is the strong correlations between different parameters: we observe that the parameter G_V is strongly correlated with all of the other parameters. The only exception is e_m^V, which is mostly uncorrelated and is essentially determined by the $\rho(770) - K^*(892) - \phi(1020)$ splitting. The correlations are summarized in Figs. 8 and 9 (Gaussianity is assumed). In Fig. 8 we provide the correlation between G_V and the other fit variables. One can clearly see that the parameter G_V, which rules the $\rho - \pi\pi$ interaction vertex in the chiral limit, is highly correlated with almost all the other parameters. By observing these plots, one can easily understand why we have obtained such different values for $L_5^{\chi\mathrm{PT}}$ in Eqs. (54) [with G_V constrained through Eq. (53)] and (56) (free G_V): the values for G_V are very different in the two fits and a positive (negative) $L_5^{\chi\mathrm{PT}}$ requires a small (large) value for G_V (see bottom-center panel in Fig. 8).

In the top left panel in Fig. 9, one can clearly observe an evident anticorrelation between F_0 and $L_4^{\chi\mathrm{PT}}$, noticed in previous works [22,62]. In addition, we observe a strong anticorrelation for $L_4^{\chi\mathrm{PT}} - c_m$ and an obvious correlation for $L_5^{\chi\mathrm{PT}} - e_m^S$, as shown in the two panels in the bottom row of Fig. 9. In Ref. [61], a lower bound on the value of $L_4^{\chi\mathrm{PT}}$ has been proposed by requiring that the pNGB decay constant in the $SU(3)$ chiral limit must be smaller than the decay constant in the $SU(2)$ limit. This gives the inequality $L_4^{\chi\mathrm{PT}} > -0.4 \times 10^{-3}$ for $\mu = 770$ MeV [22]. It is interesting to point out that this lower bound from $L_4^{\chi\mathrm{PT}}$ leads to lower or upper bounds for some of the parameters considered in our work because of the strong correlations. This can be roughly read from Figs. 8 and 9: $G_V < 72$ MeV, $F_0 < 86$ MeV, and $c_m < 68$ MeV. On the other hand, one can observe in Figs. 8 and 9 that in order to have a positive $L_5^{\chi\mathrm{PT}}$ one has the rough bounds $G_V < 60$ MeV and $e_m^S > -0.45$. Combining the paramagnetic inequality for $L_4^{\chi\mathrm{PT}}$ [22,61] and the phenomenological bound $L_5^{\chi\mathrm{PT}} > 0$ leads to the rough estimates $F_0 < 86$ MeV, $G_V < 60$ MeV, $c_m < 68$ MeV, and $e_m^S > -0.45$.

In order to further test the relations between G_V and other parameters, we want to see the impact of including a second scalar nonet. The contributions from the second scalar nonet to the decay constants in Appendix C and the matching conditions in Eqs. (42)–(44) share the same expressions as the lowest scalar multiplet, but with obvious replacements of the couplings c_d, c_m, e_m^S by c_d', c_m', and $e_m^{S'}$.

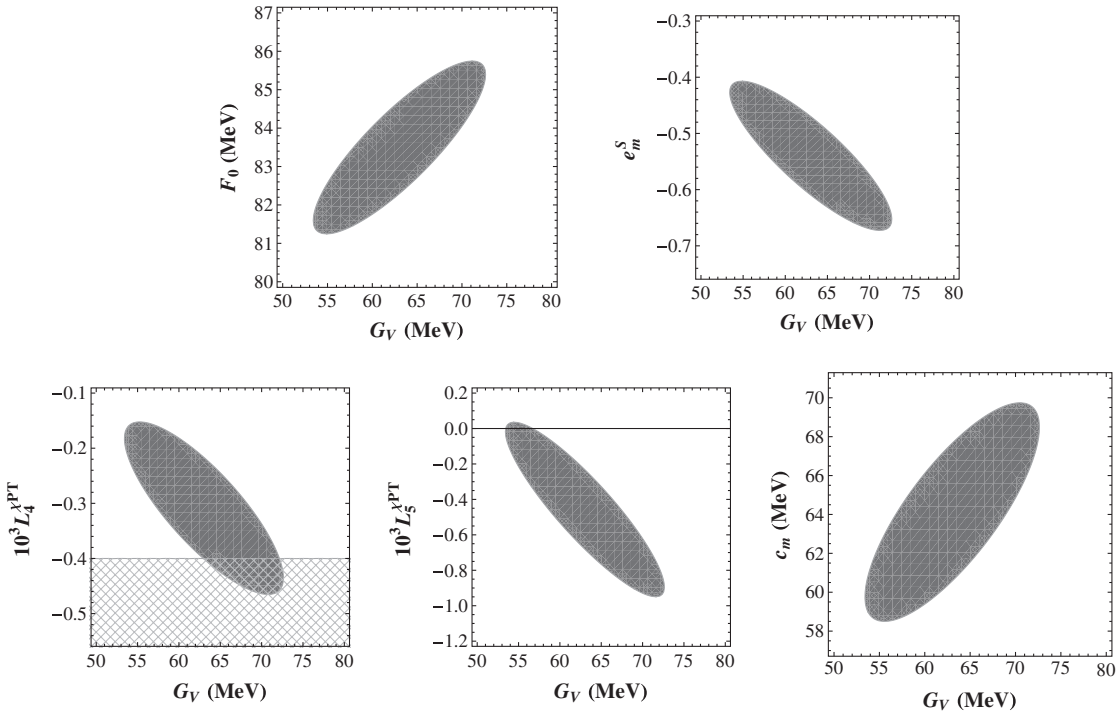

FIG. 8. 68% CL regions for G_V and other parameters. All these plots correspond to the 7-parameter analysis in Eq. (56), where G_V is also fitted.

The chiral limit resonance mass $M_{S'}$ of the excited nonet S' should be replaced as well. The introduction of the second scalar nonet will also affect the high energy constraints in Eqs. (52) and (53), which now become [44,56]

$$c_d = \frac{F_0^2 - 4c'_d c'_m}{4c_m}, \tag{58}$$

$$G_V = \sqrt{\frac{F_0^2 - 2c_d^2 - 2c_d'^2}{3}}. \tag{59}$$

Phenomenologically, the S' parameters are poorly known in the literature and we do not expect to obtain precise values from our analysis. In order to perform our quantitative estimate of the role of the second scalar nonet, we take the part of the outcomes from Ref. [63] as inputs. More precisely, we take $c'_m = c'_d$ and $M_{S'} = 2.57$ GeV (preferred fit values from Ref. [63], Eq. (6.10) therein).[4] The mass splitting parameter $e_m^{S'}$ is even worse known than c'_d and c'_m. In our rough analysis we will set its value to zero. Thus, we only have one free parameter c'_d from the second scalar nonet. In Refs. [44,63], c'_d was obtained through the constraint $F_0^2 = 4(c_d c_m + c'_d c'_m)$ by using $F_0 = F_\pi = 92.4$ MeV, whereas in our work F_0 is truly the pion decay constant in the chiral limit. Hence, instead of taking the result of c'_d from Ref. [63], we fit its value together with the chiral coupling F_0.

The fit result with the new constraints in Eqs. (58) and (59) (two scalar multiplets) turn out to be quite similar to the outcomes in Eq. (54) with only one scalar nonet in the high-energy constraints (52) and (53). The additional coupling becomes $c'_d \simeq (11 \pm 30)$ MeV, a value compatible with the preferred determination in Ref. [63] and alternative fits therein. In this work we reconfirm the large uncertainty for c'_d obtained from $K\pi$ scattering [63]. We have also tried other fits where high-energy relation (59) is released and G_V is freed and fitted. The $\rho - \pi\pi$ coupling has been also set in later fits to the particular values $G_V = F_0/\sqrt{2}$ [64] and $G_V = F_0/\sqrt{3}$ [29,56]. In all these cases the results tend to produce small central values for c'_d but with large uncertainties. As a result, the inclusion of the second scalar nonet barely changes our conclusions derived previously with only one scalar nonet.

In summary, the present determination for F_0, the $n_f = 3$ pNGB decay constant in the chiral limit, is rather stable, ranging from 78 to 86 MeV for any value of G_V in the range $40 \sim 70$ MeV. Our current determinations of the χPT LECs $L_4^{\chi PT}$ and $L_5^{\chi PT}$ cannot be pinned down to a precise range due to their strong correlations with the resonance

[4]We point out that the constraints $c_m = c_d$ and $c'_m = c'_d$ in Ref. [44] are obtained by considering the linear quark mass corrections in the minimal RχT framework (only operators with one resonance field). These two constraints do not hold any more if general RχT operators with any number of resonance fields [41] are included in the Lagrangian. This is the reason why we do not impose the constraint $c_m = c_d$ in our previous discussion with only the lightest scalar nonet. We will nevertheless employ the relation $c'_m = c'_d$ in our numerical estimate in order to stabilize the fit with two scalar nonets and to get a general idea of the impact of the second scalar multiplet.

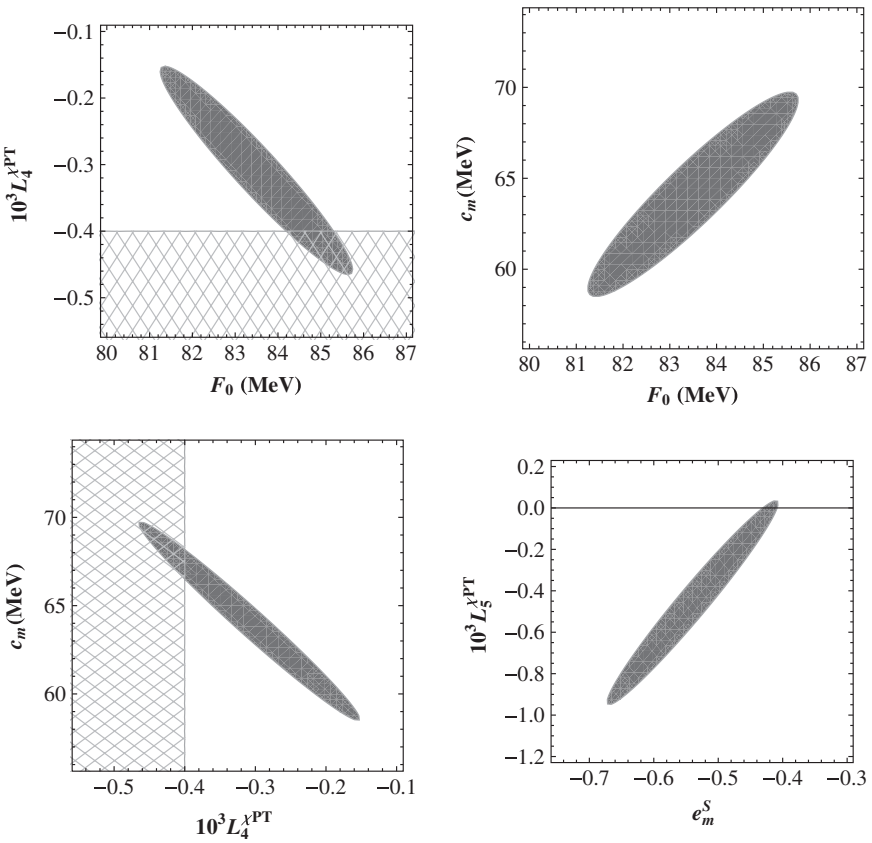

FIG. 9. 68% CL regions for sets of two couplings. All these plots correspond to the 7-parameter analysis in Eq. (56), where G_V is also fitted.

couplings, which are typically determined through some phenomenological processes with non-negligible uncertainties. Among the various resonance couplings, G_V turns out to be the crucial one to prevent us from making precise determinations. In the case of imposing the high energy constraint on G_V from Eq. (53), obtained from the discussion of the partial wave $\pi\pi$ scattering at LO in $1/N_C$ [56], the corresponding fit results in Eq. (54) are more or less compatible with the state-of-art determinations of the χPT LECs. We regard these results as our preferred ones in this work. Nonetheless, one should always bear in mind the strong correlations shown in Figs. 8 and 9.

V. CONCLUSIONS

The aim of this work is to provide a first quantitative test of the potentiality of these type of hadronic observables, such as the pNGB decay constants, for the study of resonance properties. We have calculated the pion and kaon weak decay constants within the framework of RχT up to NLO in $1/N_C$, this is, up to the one-loop level. In addition to the octet of light pNGB, we have explicitly included the singlet η_1 and the lightest vector and scalar resonance multiplets surviving at large N_C. However, we want to remark that the errors provided here should be considered with quite some care, as we have combined data from various simulation groups, ignoring correlations and systematic and lattice spacing uncertainties.

Our one-loop expressions for F_π and F_K in RχT have been properly matched to $SU(3)$ χPT up to $\mathcal{O}(p^4)$ in the small quark mass regime, providing prediction for the chiral LECs in terms of the RχT parameters. As higher order corrections from χPT are partly incorporated through the resonance loops, the present calculation provides an alternative approach which complements previous χPT analyses [21–23,65]. The price to pay in the latter is, however, the vast amount of χPT couplings one needs to consider in the full $\mathcal{O}(p^6)$ expression. In our work, the resonances are assumed to play a crucial role instead, ruling the dynamics of the decay constant.

We have extended the work from Ref. [20] (which incorporated the scalar effects at one loop) by considering also the impact of vector resonances in the loops. One of the fundamental conclusions in our study is that the vectors play a crucial role in the one-loop decay constant, being crucial parameters such as F_0, $L_4^{\chi PT}$, and $L_5^{\chi PT}$ very correlated with the value of the $\rho-\pi\pi$ coupling G_V. Low values of G_V, around 40 MeV, lead to larger values of $L_4^{\chi PT}$ and $L_5^{\chi PT}$, in closer agreement with standard χPT determinations [5]. Due to the $L_4^{\chi PT}\leftrightarrow F_0$ anticorrelation this yields a small value for F_0, around 80 MeV. On the

other hand, a G_V coupling in the range $60 \sim 70$ MeV seems to be in better agreement with vector resonance phenomenology [7,27,42,56] but generates a far too negative value for both $L_4^{\chi\mathrm{PT}}$ and $L_5^{\chi\mathrm{PT}}$, in clear contradiction with χPT determinations [5] and QCD paramagnetic inequalities [61] ($L_4^{\chi\mathrm{PT}} > -0.4 \times 10^{-3}$ for $\mu = 770$ MeV [22]). Nonetheless, in spite of this big effect on the $\mathcal{O}(p^4)$ LECs, F_0 happens to be very stable and only rises up to roughly 85 MeV. Clearly, this interplay between vector resonance loops and χPT loops deserves further investigation in future works.

In the fit where G_V is fixed to 40, 50, 60, and 70 MeV we observe clearly how the coupling F_0 evolves from 80 up to 85 MeV. Although the upper value is compatible with recent $\mathcal{O}(p^6)$ estimates [22], other analyses favor values of F_0 below 80 MeV [65]. In general, there is no agreement yet (see FLAG's review [1] and references therein) and the strong anticorrelation between F_0 and $L_4^{\chi\mathrm{PT}}$ found here and in previous works [5,22] transfers this uncertainty to the $\mathcal{O}(p^4)$ LEC $L_4^{\chi\mathrm{PT}}$.

The analysis of F_π, F_K [15–18] and F_K/F_π [19] was carried out in combination with a study of the quark mass dependence of the $\rho(770)$, η and η' masses. The simple quark mass dependence of the vector multiplet mass introduced through e_m^V perfectly accommodates the M_ρ lattice data [46–49] and the observed splitting of the physical vector multiplet [59] (Fig. 5). Likewise, the LO prediction for the $\eta - \eta'$ mixing is found to be in reasonable agreement with lattice data [51–55] (Fig. 4). We find that our theoretical formulas can reproduce the lattice data from the physical pion mass up to roughly $m_\pi = 700$ MeV. This result gives support to the linear relation between the pNGB and quark masses from Eqs. (49) and (50), assumed all along in the article.

Based on the promising fact that the present framework performs a reasonable chiral extrapolation for F_π and F_K within a broad range of pion masses, a similar study on the masses of π, K, or even η and η' should be pursued within RχT up to NLO in $1/N_C$. This would also allow us to go beyond the linear quark mass dependence considered for the squared masses of the pion and kaon in this article. We think this might help to set further and more stringent constraints on the low energy constants of the χPT Lagrangian.

ACKNOWLEDGMENTS

We would like to thank Alberto Ramos and Pere Masjuan for useful discussions, specially on the detailed explanations of the lattice simulation data. This work is partially funded by the grants National Natural Science Foundation of China (NSFC) under Contract No. 11105038, Natural Science Foundation of Hebei Province with Contract No. A2011205093, Doctor Foundation of Hebei Normal University with Contract No. L2010B04, the Spanish Government and ERDF funds from the European Commission [FPA2010-17747, SEV-2012-0249, CSD2007-00042] and the Comunidad de Madrid [HEPHACOS S2009/ESP-1473].

APPENDIX A: FEYNMAN INTEGRALS

The explicit expressions for the loop functions used in this work are given by

$$
\begin{aligned}
A_0(m^2) &= \int \frac{d^dk}{(2\pi)^d}\frac{1}{k^2-m^2} = \frac{i}{16\pi^2}m^2\left(\frac{1}{\hat{\epsilon}} - \ln\frac{m^2}{\mu^2}\right),\\
B_0(q^2,M^2,m^2) &= \int \frac{d^dk}{(2\pi)^d}\frac{1}{(k^2-m^2)((q-k)^2-M^2)} = \frac{i}{16\pi^2}\left[\frac{1}{\hat{\epsilon}} + 1 - \frac{1}{2}\ln\frac{M^2m^2}{\mu^4} + \frac{\Delta}{2s}\ln\frac{m^2}{M^2} - \frac{\nu}{2s}\ln\frac{(\Sigma - s - \nu)^2}{4M^2m^2}\right],\\
B_0'(s,M^2,m^2) &= \frac{dB_0(s,M,m)}{ds} = \frac{i}{16\pi^2}\left[-\frac{\Delta}{2s^2}\ln\frac{m^2}{M^2} - \frac{1}{s} + \frac{\Delta^2 - \Sigma s}{2\nu s^2}\ln\frac{(\Sigma - s - \nu)^2}{4M^2m^2}\right],
\end{aligned}
\tag{A1}
$$

where

$$
\begin{aligned}
&\frac{1}{\hat{\epsilon}} = \mu^{-2\epsilon}\left(\frac{1}{\epsilon} - \gamma_E + \ln 4\pi + 1\right) = \frac{1}{\epsilon} - \gamma_E + \ln 4\pi + 1 - \ln\mu^2 + \mathcal{O}(\epsilon), \qquad \left(\epsilon = 2 - \frac{D}{2}\right),\\
&\Delta = M^2 - m^2, \qquad \Sigma = M^2 + m^2, \qquad \nu = \sqrt{[s-(M+m)^2][s-(M-m)^2]}.
\end{aligned}
\tag{A2}
$$

APPENDIX B: $\eta_1 - \eta_8$ MIXING

After the diagonalization of $\eta_1 - \eta_8$ at leading order, we have the physical η and η' states at this order and their masses and the mixing angle can be found in many references in literature, such as Ref. [29]. We give the explicit formulas for the sake of completeness

$$m_\eta^2 = \frac{M_0^2}{2} + m_K^2 - \frac{\sqrt{M_0^4 - \frac{4M_0^2\Delta^2}{3} + 4\Delta^4}}{2}, \quad \text{(B1)}$$

$$m_{\eta'}^2 = \frac{M_0^2}{2} + m_K^2 + \frac{\sqrt{M_0^4 - \frac{4M_0^2\Delta^2}{3} + 4\Delta^4}}{2}, \quad \text{(B2)}$$

$$\sin\theta = -\left(\sqrt{1 + \frac{(3M_0^2 - 2\Delta^2 + \sqrt{9M_0^4 - 12M_0^2\Delta^2 + 36\Delta^4})^2}{32\Delta^4}}\right)^{-1}, \quad \text{(B3)}$$

with $\Delta^2 = m_K^2 - m_\pi^2$. Notice that m_η, $m_{\eta'}$, and θ are fully determined at this order by m_π, m_K, and M_0.

In the ideal mixing case ($M_0 = 0$) one gets $m_\eta^2 = m_\pi^2$, $m_{\eta'}^2 = 2m_K^2 - m_\pi^2$, and $\sin\theta = -\sqrt{2/3}$. On the other hand, in the chiral limit $m_\pi, m_K \to 0$ the physical masses and mixing become $m_\eta^2 = 0$, $m_{\eta'}^2 = M_0^2$, and $\theta = 0$.

APPENDIX C: FEYNMAN DIAGRAMS UP TO NLO IN $1/N_C$

1. The pion self-energy

As shown in Fig. 2, there are three types of Feynman diagrams contributing to the pNGB self-energy Σ^π. For the diagram (a) in this figure, the explicit calculation from Lagrangian in Eq. (20) leads to

$$\Sigma^{\pi-a} = \left(1 - \frac{\tilde{F}^2}{F_0^2}\right)p^2 - \left(1 - \frac{\hat{F}^2}{F_0^2}\right)m_\pi^2 + \frac{4\tilde{L}_{12}}{F_0^2}(p^2 - m_\pi^2)^2 - \frac{8\tilde{L}_{11}}{F_0^2}m_\pi^2(p^2 - m_\pi^2)$$
$$- \frac{8\tilde{L}_4}{F_0^2}(2m_K^2 + m_\pi^2)p^2 - \frac{8}{F_0^2}\left(\tilde{L}_5 + \frac{c_d c_m}{M_S^2}\right)m_\pi^2 p^2 + \frac{16\tilde{L}_6}{F_0^2}(2m_K^2 + m_\pi^2)m_\pi^2 + \frac{16}{F_0^2}\left(\tilde{L}_8 + \frac{c_m^2}{2M_S^2}\right)m_\pi^4, \quad \text{(C1)}$$

where we have used the linear relations (49) and (50) to rewrite the quark masses in terms of the pion and kaon masses. The tree-level contributions from the operators in the second line of Eq. (24) have also been taken into account.

About the diagram (b) in Fig. 2, its contribution to the pion self-energy is the same as in $U(3)$ χPT, which is calculated by using leading order Lagrangian in Eq. (13) and reads

$$\Sigma^{\pi-b} = \frac{i}{3F_0^2}\left(2p^2 - \frac{m_\pi^2}{2}\right)A_0(m_\pi^2) + \frac{i}{3F_0^2}(p^2 - m_\pi^2)A_0(m_K^2) + \frac{-i}{2F_0^2}\frac{(c_\theta - \sqrt{2}s_\theta)^2}{3}m_\pi^2 A_0(m_\eta^2) + \frac{-i}{2F_0^2}\frac{(\sqrt{2}c_\theta + s_\theta)^2}{3}m_\pi^2 A_0(m_{\eta'}^2). \quad \text{(C2)}$$

The diagram (c) in Fig. 2 receives contributions both from scalar and vector resonances. Let us take the self-energy for the π^- for illustration. There are five possible combinations of scalar resonance and pseudoscalar meson running inside the loop: $\sigma\pi^-$, $\kappa^- K^0$, $\kappa^0 K^-$, $a_0^-\eta$, and $a_0^-\eta'$, which will be labeled as $-i\Sigma^{\pi-cSj}$, with $j = 1, 2, 3, 4, 5$, respectively. About the vector, there are four possible combinations: $\rho^-\pi^0$, $\rho^0\pi^-$, $K^{*0}K^-$, and $K^{*-}K^0$, which will be labeled as $-i\Sigma^{\pi-cVj}$, with $j = 1, 2, 3, 4$, respectively.

The explicit results of $\Sigma^{\pi-cSj}$ for $j = 1, 2, 3, 4, 5$ are

$$\Sigma^{\pi-cS1} = \frac{i2c_d^2}{F_0^4}[(3p^2 + m_\pi^2 - M_\sigma^2)A_0(M_\sigma^2) - (m_\pi^2 + p^2 - M_\sigma^2)A_0(m_\pi^2) + (m_\pi^2 + p^2 - M_\sigma^2)^2 B_0(p^2, M_\sigma^2, m_\pi^2)]$$
$$- \frac{i8c_d c_m}{F_0^4 M_S^2}m_\pi^2 M_\sigma^2[(m_\pi^2 + p^2 - M_\sigma^2)B_0(p^2, M_\sigma^2, m_\pi^2) + A_0(M_\sigma^2) - A_0(m_\pi^2)]$$
$$+ \frac{i8c_m^2}{F_0^4 M_S^4}m_\pi^4[M_\sigma^4 B_0(p^2, M_\sigma^2, m_\pi^2) + (m_\pi^2 + p^2 + M_\sigma^2)A_0(m_\pi^2)], \quad \text{(C3)}$$

$$\Sigma^{\pi-cS2} = \Sigma^{\pi-cS3} = \frac{ic_d^2}{F_0^4}[(3p^2 + m_K^2 - M_\kappa^2)A_0(M_\kappa^2) - (m_K^2 + p^2 - M_\kappa^2)A_0(m_K^2) + (m_K^2 + p^2 - M_\kappa^2)^2 B_0(p^2, M_\kappa^2, m_K^2)]$$
$$- \frac{i2c_d c_m}{F_0^4 M_S^2}\{[2m_\pi^2 M_\kappa^2 + (m_K^2 - m_\pi^2)(M_\kappa^2 - s - m_K^2)]A_0(M_\kappa^2) + [-2m_\pi^2 M_\kappa^2 + (m_K^2 - m_\pi^2)(m_K^2 - s - M_\kappa^2)]A_0(m_K^2)$$
$$+ [2m_\pi^2 M_\kappa^2(s + m_K^2 - M_\kappa^2) + (m_K^2 - m_\pi^2)(s^2 - M_\kappa^4 - m_K^4 + 2m_K^2 M_\kappa^2)]B_0(p^2, M_\kappa^2, m_K^2)\}$$

$$+\frac{ic_m^2}{F_0^4M_S^4}\{[-4m_\pi^2(m_K^2-m_\pi^2)M_\kappa^2+(m_K^2-m_\pi^2)^2(m_K^2-s-M_\kappa^2)]A_0(M_\kappa^2)$$
$$+[4m_\pi^4(s+m_K^2+M_\kappa^2)+4m_\pi^2(m_K^2-m_\pi^2)(2s+M_\kappa^2)+(m_K^2-m_\pi^2)^2(3s+M_\kappa^2-m_K^2)]A_0(m_K^2)$$
$$+[4m_\pi^4M_\kappa^4+4m_\pi^2(m_K^2-m_\pi^2)(s+M_\kappa^2-m_K^2)M_\kappa^2+(m_K^2-m_\pi^2)^2(s+M_\kappa^2-m_K^2)^2]B_0(p^2,M_\kappa^2,m_K^2)\},\tag{C4}$$

$$\Sigma^{\pi-cS4}=\frac{(c_\theta-\sqrt{2}s_\theta)^2}{3}\left\{\frac{i2c_d^2}{F_0^4}[(3p^2+m_\eta^2-M_a^2)A_0(M_a^2)-(m_\eta^2+p^2-M_a^2)A_0(m_\eta^2)+(m_\eta^2+p^2-M_a^2)^2B_0(p^2,M_a^2,m_\eta^2)]\right.$$
$$-\frac{i8c_dc_m}{F_0^4M_S^2}m_\pi^2M_a^2[(m_\eta^2+p^2-M_a^2)B_0(p^2,M_a^2,m_\eta^2)+A_0(M_a^2)-A_0(m_\eta^2)]$$
$$\left.+\frac{i8c_m^2}{F_0^4M_S^4}m_\pi^4[M_a^4B_0(p^2,M_a^2,m_\eta^2)+(m_\eta^2+p^2+M_a^2)A_0(m_\eta^2)]\right\},\tag{C5}$$

$$\Sigma^{\pi-cS5}=\frac{(\sqrt{2}c_\theta+s_\theta)^2}{3}\left\{\frac{i2c_d^2}{F_0^4}[(3p^2+m_{\eta'}^2-M_a^2)A_0(M_a^2)-(m_{\eta'}^2+p^2-M_a^2)A_0(m_{\eta'}^2)+(m_{\eta'}^2+p^2-M_a^2)^2B_0(p^2,M_a^2,m_{\eta'}^2)]\right.$$
$$-\frac{i8c_dc_m}{F_0^4M_S^2}m_\pi^2M_a^2[(m_{\eta'}^2+p^2-M_a^2)B_0(p^2,M_a^2,m_{\eta'}^2)+A_0(M_a^2)-A_0(m_{\eta'}^2)]$$
$$\left.+\frac{i8c_m^2}{F_0^4M_S^4}m_\pi^4[M_a^4B_0(p^2,M_a^2,m_{\eta'}^2)+(m_{\eta'}^2+p^2+M_a^2)A_0(m_{\eta'}^2)]\right\}.\tag{C6}$$

For the vector contributions, we have

$$\Sigma^{\pi-cV1}=\Sigma^{\pi-cV2}=\frac{iG_V^2}{F_0^4}\{-(p^2-m_\pi^2+M_\rho^2)A_0(M_\rho^2)-(p^2+m_\pi^2-M_\rho^2)A_0(m_\pi^2)$$
$$+[(p^2-m_\pi^2+M_\rho^2)^2-4p^2M_\rho^2]B_0(p^2,M_\rho^2,m_\pi^2)\},\tag{C7}$$

$$\Sigma^{\pi-cV3}=\Sigma^{\pi-cV4}=\frac{iG_V^2}{2F_0^4}\{-(p^2-m_K^2+M_{K^*}^2)A_0(M_{K^*}^2)-(p^2+m_K^2-M_{K^*}^2)A_0(m_K^2)$$
$$+[(p^2-m_K^2+M_{K^*}^2)^2-4p^2M_{K^*}^2]B_0(p^2,M_{K^*}^2,m_K^2)\}.\tag{C8}$$

2. The kaon self-energy

The calculation of the kaon self-energy is similar to the pion case. The corresponding self-energy function from the type (a) diagram in Fig. 2 is

$$\Sigma^{K-a}=\left(1-\frac{\tilde{F}^2}{F_0^2}\right)p^2-\left(1-\frac{\hat{F}^2}{F_0^2}\right)m_K^2+\frac{4\tilde{L}_{12}}{F_0^2}(p^2-m_K^2)^2$$
$$-\frac{8\tilde{L}_{11}}{F_0^2}m_K^2(p^2-m_K^2)-\frac{8\tilde{L}_4}{F_0^2}(2m_K^2+m_\pi^2)p^2$$
$$-\frac{8}{F_0^2}\left(\tilde{L}_5+\frac{c_dc_m}{M_S^2}\right)m_K^2p^2+\frac{16\tilde{L}_6}{F_0^2}(2m_K^2+m_\pi^2)m_K^2$$
$$+\frac{16}{F_0^2}\left(\tilde{L}_8+\frac{c_m^2}{2M_S^2}\right)m_K^4,\tag{C9}$$

where we have used the linear relations (49) and (50) to rewrite the quark masses in terms of the pion and kaon masses.

Again, the diagram (b) in Fig. 2 leads to the same results as in $U(3)$ χPT, which is given by

$$\Sigma^{K-b}=\frac{i}{2F_0^2}(p^2-m_K^2)A_0(m_K^2)+\frac{i}{4F_0^2}(p^2-m_K^2)A_0(m_\pi^2)$$
$$+\frac{i}{12F_0^2}\{3c_\theta^2(p^2+m_\eta^2)-[(3c_\theta^2+4\sqrt{2}c_\theta s_\theta+4s_\theta^2)m_K^2$$
$$-(c_\theta^2+2\sqrt{2}c_\theta s_\theta)m_\pi^2]\}A_0(m_\eta^2)$$
$$+\frac{i}{6F_0^2}\left\{\frac{3s_\theta^2}{2}(p^2+m_{\eta'}^2)-\frac{1}{2}[(4c_\theta^2-4\sqrt{2}c_\theta s_\theta+3s_\theta^2)m_K^2\right.$$
$$\left.+(2\sqrt{2}c_\theta s_\theta-s_\theta^2)m_\pi^2]\right\}A_0(m_{\eta'}^2).\tag{C10}$$

About the diagram (c) in Fig. 2, let us take the self-energy for the K^- for illustration purposes. There are eight possible combinations of scalar resonance and pseudoscalar meson running inside the loop: σK^-, $\sigma' K^-$, $a_0^0 K^-$, $a_0^- \bar{K}^0$, $\kappa^- \pi^0$, $\kappa^0 \pi^-$, $\kappa^- \eta$, and $\kappa^- \eta'$, which will be labeled as $-i\Sigma^{K-cSj}$, with $j = 1, 2, 3, 4, 5, 6, 7, 8$, respectively. For the vector case, there are also eight possible combinations: $\rho^0 K^-$, $\rho^- \bar{K}^0$, ωK^-, ϕK^-, $K^{*-}\pi^0$, $\bar{K}^{*0}\pi^-$, $K^{*-}\eta$, and $K^{*-}\eta'$, which will be labeled as $-i\Sigma^{K-cVj}$, with $j = 1, 2, 3, 4, 5, 6, 7, 8$, respectively. The final results read

$$\begin{aligned}\Sigma^{K-cS1} &= \frac{ic_d^2}{2F_0^4}[(3p^2 + m_K^2 - M_\sigma^2)A_0(M_\sigma^2) - (p^2 + m_K^2 - M_\sigma^2)A_0(m_K^2) + (p^2 + m_K^2 - M_\sigma^2)^2 B_0(p^2, M_\sigma^2, m_K^2)] \\ &\quad - \frac{i2c_d c_m}{F_0^4 M_S^2} m_K^2 M_\sigma^2 [(m_K^2 + p^2 - M_\sigma^2)B_0(p^2, M_\sigma^2, m_K^2) + A_0(M_\sigma^2) - A_0(m_K^2)] \\ &\quad + \frac{i2c_m^2}{F_0^4 M_S^4} m_K^4 [M_\sigma^4 B_0(p^2, M_\sigma^2, m_K^2) + (m_K^2 + p^2 + M_\sigma^2)A_0(m_K^2)], \end{aligned} \tag{C11}$$

$$\begin{aligned}\Sigma^{K-cS2} &= \frac{ic_d^2}{F_0^4}[(3p^2 + m_K^2 - M_{\sigma'}^2)A_0(M_{\sigma'}^2) - (p^2 + m_K^2 - M_{\sigma'}^2)A_0(m_K^2) + (p^2 + m_K^2 - M_{\sigma'}^2)^2 B_0(p^2, M_{\sigma'}^2, m_K^2)] \\ &\quad - \frac{i4c_d c_m}{F_0^4 M_S^2} m_K^2 M_{\sigma'}^2 [(m_K^2 + p^2 - M_{\sigma'}^2)B_0(p^2, M_{\sigma'}^2, m_K^2) + A_0(M_{\sigma'}^2) - A_0(m_K^2)] \\ &\quad + \frac{i4c_m^2}{F_0^4 M_S^4} m_K^4 [M_{\sigma'}^4 B_0(p^2, M_{\sigma'}^2, m_K^2) + (m_K^2 + p^2 + M_{\sigma'}^2)A_0(m_K^2)], \end{aligned} \tag{C12}$$

$$\begin{aligned}\Sigma^{K-cS4} = 2\Sigma^{K-cS3} &= \frac{ic_d^2}{F_0^4}[(3p^2 + m_K^2 - M_a^2)A_0(M_a^2) - (p^2 + m_K^2 - M_a^2)A_0(m_K^2) + (p^2 + m_K^2 - M_a^2)^2 B_0(p^2, M_a^2, m_K)] \\ &\quad - \frac{i4c_d c_m}{F_0^4 M_S^2} m_K^2 M_a^2 [(m_K^2 + p^2 - M_a^2)B_0(p^2, M_a^2, m_K^2) + A_0(M_a^2) - A_0(m_K^2)] \\ &\quad + \frac{i4c_m^2}{F_0^4 M_S^4} m_K^4 [M_a^4 B_0(p^2, M_a^2, m_K^2) + (m_K^2 + p^2 + M_a^2)A_0(m_K^2)], \end{aligned} \tag{C13}$$

$$\begin{aligned}\Sigma^{K-cS6} = 2\Sigma^{K-cS5} &= \frac{ic_d^2}{F_0^4}[(3p^2 + m_\pi^2 - M_\kappa^2)A_0(M_\kappa^2) - (p^2 + m_\pi^2 - M_\kappa^2)A_0(m_\pi^2) + (p^2 + m_\pi^2 - M_\kappa^2)^2 B_0(p^2, M_\kappa^2, m_\pi)] \\ &\quad - \frac{i2c_d c_m}{F_0^4 M_S^2} \{[2m_K^2 M_\kappa^2 - (m_K^2 - m_\pi^2)(M_\kappa^2 - s - m_\pi^2)]A_0(M_\kappa^2) + [-2m_K^2 M_\kappa^2 - (m_K^2 - m_\pi^2)(m_\pi^2 - s - M_\kappa^2)]A_0(m_\pi^2) \\ &\quad + [2m_K^2 M_\kappa^2(s + m_\pi^2 - M_\kappa^2) - (m_K^2 - m_\pi^2)(s^2 - M_\kappa^4 - m_\pi^4 + 2m_\pi^2 M_\kappa^2)]B_0(p^2, M_\kappa^2, m_\pi^2)\} \\ &\quad + \frac{ic_m^2}{F_0^4 M_S^4} \{[4m_K^2(m_K^2 - m_\pi^2)M_\kappa^2 + (m_K^2 - m_\pi^2)^2(m_\pi^2 - s - M_\kappa^2)]A_0(M_\kappa^2) \\ &\quad + [4m_K^4(s + m_\pi^2 + M_\kappa^2) - 4m_K^2(m_K^2 - m_\pi^2)(2s + M_\kappa^2) + (m_K^2 - m_\pi^2)^2(3s + M_\kappa^2 - m_\pi^2)]A_0(m_\pi^2) \\ &\quad + [4m_K^4 M_\kappa^4 - 4m_K^2(m_K^2 - m_\pi^2)(s + M_\kappa^2 - m_\pi^2)M_\kappa^2 + (m_K^2 - m_\pi^2)^2(s + M_\kappa^2 - m_\pi^2)^2]B_0(p^2, M_\kappa^2, m_\pi^2)\}, \end{aligned} \tag{C14}$$

$$\Sigma^{K-cS7}=\frac{ic_d^2}{2F_0^4}\frac{(c_\theta+2\sqrt{2}s_\theta)^2}{3}[(3p^2+m_\eta^2-M_\kappa^2)A_0(M_\kappa^2)-(p^2+m_\eta^2-M_\kappa^2)A_0(m_\eta^2)+(p^2+m_\eta^2-M_\kappa^2)^2B_0(p^2,M_\kappa^2,m_\eta)]$$
$$-\frac{ic_dc_m}{F_0^4M_S^2}(c_\theta+2\sqrt{2}s_\theta)\Bigg\{\left[\frac{2(c_\theta+2\sqrt{2}s_\theta)}{3}m_K^2M_\kappa^2+c_\theta(m_K^2-m_\pi^2)(M_\kappa^2-s-m_\eta^2)\right]A_0(M_\kappa^2)$$
$$+\left[-\frac{2(c_\theta+2\sqrt{2}s_\theta)}{3}m_K^2M_\kappa^2+c_\theta(m_K^2-m_\pi^2)(m_\eta^2-s-M_\kappa^2)\right]A_0(M_\eta)$$
$$+\left[\frac{2(c_\theta+2\sqrt{2}s_\theta)}{3}m_K^2(s+m_\eta^2-M_\kappa^2)M_\kappa^2+c_\theta(m_K^2-m_\pi^2)(s^2-m_\eta^4-M_\kappa^4+2m_\eta^2M_\kappa^2)\right]B_0(p^2,M_\kappa^2,m_\eta^2)\Bigg\}$$
$$+\frac{ic_m^2}{F_0^4M_S^4}\Bigg\{[-2(c_\theta+2\sqrt{2}s_\theta)c_\theta m_K^2(m_K^2-m_\pi^2)M_\kappa^2+\frac{3}{2}c_\theta^2(m_K^2-m_\pi^2)^2(m_\eta^2-s-M_\kappa^2)]A_0(M_\kappa^2)$$
$$+\left[\frac{2(c_\theta+2\sqrt{2}s_\theta)^2}{3}m_K^4(s+m_\eta^2+M_\kappa^2)+2(c_\theta+2\sqrt{2}s_\theta)c_\theta m_K^2(m_K^2-m_\pi^2)(2s+M_\kappa^2)\right.$$
$$\left.+\frac{3}{2}c_\theta^2(m_K^2-m_\pi^2)^2(3s+M_\kappa^2-m_\eta^2)\right]A_0(M_\eta)+\left[\frac{2(c_\theta+2\sqrt{2}s_\theta)^2}{3}m_K^4M_\kappa^4\right.$$
$$\left.+2(c_\theta+2\sqrt{2}s_\theta)c_\theta m_K^2(m_K^2-m_\pi^2)(s+M_\kappa^2-m_\eta^2)M_\kappa^2+\frac{3}{2}c_\theta^2(m_K^2-m_\pi^2)^2(s+M_\kappa^2-m_\eta^2)^2\right]B_0(p^2,M_\kappa^2,m_\eta^2)\Bigg\},\quad\text{(C15)}$$

$$\Sigma^{K-cS8}=\frac{ic_d^2}{F_0^4}\frac{(2\sqrt{2}c_\theta-s_\theta)^2}{6}[(3p^2+m_{\eta'}^2-M_\kappa^2)A_0(M_\kappa^2)-(p^2+m_{\eta'}^2-M_\kappa^2)A_0(m_{\eta'}^2)+(p^2+m_{\eta'}^2-M_\kappa^2)^2B_0(p^2,M_\kappa^2,m_{\eta'})]$$
$$+\frac{ic_dc_m}{F_0^4M_S^2}(2\sqrt{2}c_\theta-s_\theta)\Bigg\{\left[\frac{2(s_\theta-2\sqrt{2}c_\theta)}{3}m_K^2M_\kappa^2+s_\theta(m_K^2-m_\pi^2)(M_\kappa^2-s-m_{\eta'}^2)\right]A_0(M_\kappa^2)$$
$$+\left[-\frac{2(s_\theta-2\sqrt{2}c_\theta)}{3}m_K^2M_\kappa^2+s_\theta(m_K^2-m_\pi^2)(m_{\eta'}^2-s-M_\kappa^2)\right]A_0(M_{\eta'})$$
$$+\left[\frac{2(s_\theta-2\sqrt{2}c_\theta)}{3}m_K^2(s+m_{\eta'}^2-M_\kappa^2)M_\kappa^2+s_\theta(m_K^2-m_\pi^2)(s^2-m_{\eta'}^4-M_\kappa^4+2m_{\eta'}^2M_\kappa^2)\right]B_0(p^2,M_\kappa^2,m_{\eta'}^2)\Bigg\}$$
$$+\frac{ic_m^2}{F_0^4M_S^4}\Bigg\{[-2(s_\theta-2\sqrt{2}c_\theta)s_\theta m_K^2(m_K^2-m_\pi^2)M_\kappa^2+\frac{3}{2}s_\theta^2(m_K^2-m_\pi^2)^2(m_{\eta'}^2-s-M_\kappa^2)]A_0(M_\kappa^2)$$
$$+\left[\frac{2(s_\theta-2\sqrt{2}c_\theta)^2}{3}m_K^4(s+m_{\eta'}^2+M_\kappa^2)+2(s_\theta-2\sqrt{2}c_\theta)s_\theta m_K^2(m_K^2-m_\pi^2)(2s+M_\kappa^2)\right.$$
$$\left.+\frac{3}{2}s_\theta^2(m_K^2-m_\pi^2)^2(3s+M_\kappa^2-m_{\eta'}^2)\right]A_0(M_{\eta'})+\left[\frac{2(s_\theta-2\sqrt{2}c_\theta)^2}{3}m_K^4M_\kappa^4\right.$$
$$\left.+2(s_\theta-2\sqrt{2}c_\theta)s_\theta m_K^2(m_K^2-m_\pi^2)(s+M_\kappa^2-m_{\eta'}^2)M_\kappa^2+\frac{3}{2}s_\theta^2(m_K^2-m_\pi^2)^2(s+M_\kappa^2-m_{\eta'}^2)^2\right]B_0(p^2,M_\kappa^2,m_{\eta'}^2)\Bigg\}.$$
(C16)

For the contributions from the vector resonances, the explicit results are

$$\Sigma^{K-cV2}=2\Sigma^{K-cV1}=\frac{iG_V^2}{2F_0^4}\{-(p^2-m_K^2+M_\rho^2)A_0(M_\rho^2)-(p^2+m_K^2-M_\rho^2)A_0(m_K^2)$$
$$+[(p^2-m_K^2+M_\rho^2)^2-4p^2M_\rho^2]B_0(p^2,M_\rho^2,m_K^2)\},\quad\text{(C17)}$$

$$\Sigma^{K-cV3}=\frac{iG_V^2}{4F_0^4}\{-(p^2-m_K^2+M_\omega^2)A_0(M_\omega^2)-(p^2+m_K^2-M_\omega^2)A_0(m_K^2)+[(p^2-m_K^2+M_\omega^2)^2-4p^2M_\omega^2]B_0(p^2,M_\omega^2,m_K^2)\}, \tag{C18}$$

$$\Sigma^{K-cV4}=\frac{iG_V^2}{2F_0^4}\{-(p^2-m_K^2+M_\phi^2)A_0(M_\phi^2)-(p^2+m_K^2-M_\phi^2)A_0(m_K^2)+[(p^2-m_K^2+M_\phi^2)^2-4p^2M_\phi^2]B_0(p^2,M_\phi^2,m_K^2)\}, \tag{C19}$$

$$\begin{aligned}\Sigma^{K-cV6}=2\Sigma^{K-cV5}=\frac{iG_V^2}{2F_0^4}\{&-(p^2-m_\pi^2+M_{K^*}^2)A_0(M_{K^*}^2)-(p^2+m_\pi^2-M_{K^*}^2)A_0(m_\pi^2)\\&+[(p^2-m_\pi^2+M_{K^*}^2)^2-4p^2M_{K^*}^2]B_0(p^2,M_{K^*}^2,m_\pi^2)\},\end{aligned} \tag{C20}$$

$$\begin{aligned}\Sigma^{K-cV7}=\frac{iG_V^2}{4F_0^4}3c_\theta^2\{&-(p^2-m_\eta^2+M_{K^*}^2)A_0(M_{K^*}^2)-(p^2+m_\eta^2-M_{K^*}^2)A_0(m_\eta^2)\\&+[(p^2-m_\eta^2+M_{K^*}^2)^2-4p^2M_{K^*}^2]B_0(p^2,M_{K^*}^2,m_\eta^2)\},\end{aligned} \tag{C21}$$

$$\begin{aligned}\Sigma^{K-cV8}=\frac{iG_V^2}{2F_0^4}\frac{3s_\theta^2}{2}\{&-(p^2-m_{\eta'}^2+M_{K^*}^2)A_0(M_{K^*}^2)-(p^2+m_{\eta'}^2-M_{K^*}^2)A_0(m_{\eta'}^2)\\&+[(p^2-m_{\eta'}^2+M_{K^*}^2)^2-4p^2M_{K^*}^2]B_0(p^2,M_{K^*}^2,m_{\eta'}^2)\}.\end{aligned} \tag{C22}$$

3. The results for F_π^{1PI} in Eq. (30)

The relevant Feynman diagrams are shown in Fig. 3 and the explicit results for those diagrams will be collected in T^ϕ, with $\phi=\pi,K$. For the diagram (a), the final expression is

$$T^{\pi-a}=\sqrt{2}F_0p_\nu\left[\frac{\tilde{F}^2}{F_0^2}-\frac{4\tilde{L}_{12}}{F_0^2}(p^2-m_\pi^2)+\frac{4\tilde{L}_{11}}{F_0^2}m_\pi^2+\frac{8\tilde{L}_4}{F_0^2}(2m_K^2+m_\pi^2)+\frac{8}{F_0^2}\left(\tilde{L}_5+\frac{c_dc_m}{M_S^2}\right)m_\pi^2\right]. \tag{C23}$$

The result from diagram (b) reads

$$T^{\pi-b}=-i\sqrt{2}F_0p_\nu\left[\frac{4}{3F_0^2}A_0(m_\pi^2)+\frac{2}{3F_0^2}A_0(m_K^2)\right], \tag{C24}$$

which is the same as in $U(3)$ χPT calculation.

The diagram (c) in Fig. 3 receives contributions both from scalar and vector resonances. Similar to the self-energy case, we take the π^- for illustration. There are five possible combinations of scalar resonance and pseudoscalar meson running inside the loop, which are exactly the same as in the self-energy calculation: $\sigma\pi^-$, κ^-K^0, κ^0K^-, $a_0^-\eta$, and $a_0^-\eta'$, which will be labeled as $T^{\pi-cSj}$, with $j=1,2,3,4,5$, respectively. About the vector, there are four possible combinations: $\rho^-\pi^0$, $\rho^0\pi^-$, $K^{*0}K^-$, and $K^{*-}K^0$, which will be labeled as $T^{\pi-cVj}$, with $j=1,2,3,4$, respectively.

The final results of these diagrams involving scalar resonances are

$$\begin{aligned}T^{\pi-cS1}=&\frac{-i2\sqrt{2}c_d^2}{F_0^3p^2}p_\nu[(3p^2+m_\pi^2-M_\sigma^2)A_0(M_\sigma^2)-(m_\pi^2+p^2-M_\sigma^2)A_0(m_\pi^2)+(m_\pi^2+p^2-M_\sigma^2)^2B_0(p^2,M_\sigma^2,m_\pi^2)]\\&+\frac{i4\sqrt{2}c_dc_m}{F_0^3M_S^2p^2}p_\nu m_\pi^2M_\sigma^2[(m_\pi^2+p^2-M_\sigma^2)B_0(p^2,M_\sigma^2,m_\pi^2)+A_0(M_\sigma^2)-A_0(m_\pi^2)],\end{aligned} \tag{C25}$$

$$T^{\pi-cS2}=T^{\pi-cS3}=\frac{-i\sqrt{2}c_d^2}{F_0^3p^2}p_\nu[(3p^2+m_K^2-M_\kappa^2)A_0(M_\kappa^2)-(m_K^2+p^2-M_\kappa^2)A_0(m_K^2)+(m_K^2+p^2-M_\kappa^2)^2B_0(p^2,M_\kappa^2,m_K^2)]$$
$$+\frac{i2\sqrt{2}c_dc_m}{F_0^3M_S^2p^2}p_\nu\{[m_\pi^2M_\kappa^2+(m_K^2-m_\pi^2)(M_\kappa^2-s-m_K^2)]A_0(M_\kappa^2)+[-m_\pi^2M_\kappa^2+(m_K^2-m_\pi^2)(m_K^2-s-M_\kappa^2)]A_0(m_K^2)$$
$$+[m_\pi^2M_\kappa^2(s+m_K^2-M_\kappa^2)+(m_K^2-m_\pi^2)(s^2-M_\kappa^4-m_K^4+2m_K^2M_\kappa^2)]B_0(p^2,M_\kappa^2,m_K^2)\}$$
$$-\frac{i\sqrt{2}c_m^2}{F_0^3M_S^4p^2}p_\nu\{[-2m_\pi^2(m_K^2-m_\pi^2)M_\kappa^2+(m_K^2-m_\pi^2)^2(m_K^2-s-M_\kappa^2)]A_0(M_\kappa^2)$$
$$+[2m_\pi^2(m_K^2-m_\pi^2)(2s+M_\kappa^2)+(m_K^2-m_\pi^2)^2(3s+M_\kappa^2-m_K^2)]A_0(m_K^2)$$
$$+[2m_\pi^2(m_K^2-m_\pi^2)(s+M_\kappa^2-m_K^2)M_\kappa^2+(m_K^2-m_\pi^2)^2(s+M_\kappa^2-m_K^2)^2]B_0(p^2,M_\kappa^2,m_K^2)\},\tag{C26}$$

$$T^{\pi-cS4}=\frac{(c_\theta-\sqrt{2}s_\theta)^2}{3}\times\frac{-i2\sqrt{2}c_d^2}{F_0^3p^2}p_\nu[(3p^2+m_\eta^2-M_a^2)A_0(M_a^2)-(m_\eta^2+p^2-M_a^2)A_0(m_\eta^2)+(m_\eta^2+p^2-M_a^2)^2B_0(p^2,M_a^2,m_\eta^2)]$$
$$+\frac{i4\sqrt{2}c_dc_m}{F_0^3M_S^2p^2}p_\nu m_\pi^2M_a^2[(m_\eta^2+p^2-M_a^2)B_0(p^2,M_a^2,m_\eta^2)+A_0(M_a^2)-A_0(m_\eta^2)],\tag{C27}$$

$$T^{\pi-cS5}=\frac{(\sqrt{2}c_\theta+s_\theta)^2}{3}\times\frac{-i2\sqrt{2}c_d^2}{F_0^3p^2}p_\nu[(3p^2+m_{\eta'}^2-M_a^2)A_0(M_a^2)-(m_{\eta'}^2+p^2-M_a^2)A_0(m_{\eta'}^2)$$
$$+(m_{\eta'}^2+p^2-M_a^2)^2B_0(p^2,M_a^2,m_{\eta'}^2)]+\frac{i4\sqrt{2}c_dc_m}{F_0^3M_S^2p^2}p_\nu m_\pi^2M_a^2[(m_{\eta'}^2+p^2-M_a^2)B_0(p^2,M_a^2,m_{\eta'}^2)+A_0(M_a^2)-A_0(m_{\eta'}^2)].\tag{C28}$$

For the vector resonances, after an explicit calculation we find that $T^{\pi-cVi}$ is directly related to the self-energy function $\Sigma^{Z\pi Vi}$ through

$$T^{\pi-cVi}=-\sqrt{2}F_0p_\nu\frac{1}{p^2}\Sigma^{Z\pi Vi},\qquad i=1,2,3,4,5.\tag{C29}$$

4. The results for F_K^{1PI} in Eq. (30)

It shares the same Feynman diagrams as F_π with different resonances and pseudoscalar mesons running inside the loops in Fig. 3. The expression for diagram (a) takes the form

$$T^{K-a}=\sqrt{2}F_0p_\nu\left[\frac{\tilde{F}^2}{F_0^2}-\frac{4\tilde{L}_{12}}{F_0^2}(p^2-m_K^2)+\frac{4\tilde{L}_{11}}{F_0^2}m_K^2\right.$$
$$\left.+\frac{8\tilde{L}_4}{F_0^2}(2m_K^2+m_\pi^2)+\frac{8}{F_0^2}\left(\tilde{L}_5+\frac{c_dc_m}{M_S^2}\right)m_K^2\right].\tag{C30}$$

About the diagram (b), its explicit result is

$$T^{K-b}=-i\sqrt{2}F_0p_\nu\left[\frac{1}{F_0^2}A_0(m_K^2)+\frac{1}{2F_0^2}A_0(m_\pi^2)\right.$$
$$\left.+\frac{c_\theta^2}{2F_0^2}A_0(m_\eta^2)+\frac{s_\theta^2}{3F_0^2}A_0(m_{\eta'}^2)\right].\tag{C31}$$

For the diagram (c) in Fig. 3, we take the self-energy for the K^- for illustrating purpose. Exactly the same as in the self-energy case, there are eight possible combinations of scalar resonance and pseudoscalar meson running inside the loop: σK^-, $\sigma' K^-$, $a_0^0K^-$, $a_0^-\bar{K}^0$, $\kappa^-\pi^0$, $\kappa^0\pi^-$, $\kappa^-\eta$, and $\kappa^-\eta'$, which will be labeled as T^{K-cSj}, with $j=1,2,3,4,5,6,7,8$, respectively. For the vector case, there are also eight possible combinations: ρ^0K^-, $\rho^-\bar{K}^0$, ωK^-, ϕK^-, $K^{*-}\pi^0$, $\bar{K}^{*0}\pi^-$, $K^{*-}\eta$, and $K^{*-}\eta'$, which will be labeled as T^{K-cVj}, with $j=1,2,3,4,5,6,7,8$, respectively. The final expressions for the diagrams involving scalar resonances are

$$T^{K-cS1}=\frac{-ic_d^2}{\sqrt{2}F_0^3p^2}p_\nu[(3p^2+m_K^2-M_\sigma^2)A_0(M_\sigma^2)-(p^2+m_K^2-M_\sigma^2)A_0(m_K^2)+(p^2+m_K^2-M_\sigma^2)^2$$
$$\times B_0(p^2,M_\sigma^2,m_K^2)]+\frac{i\sqrt{2}c_dc_m}{F_0^3M_S^2p^2}p_\nu m_K^2M_\sigma^2[(m_K^2+p^2-M_\sigma^2)B_0(p^2,M_\sigma^2,m_K^2)+A_0(M_\sigma^2)-A_0(m_K^2)],\tag{C32}$$

$$T^{K-cS2} = \frac{-i\sqrt{2}c_d^2}{F_0^3 p^2} p_\nu [(3p^2 + m_K^2 - M_{\sigma'}^2)A_0(M_{\sigma'}^2) - (p^2 + m_K^2 - M_{\sigma'}^2)A_0(m_K^2) + (p^2 + m_K^2 - M_{\sigma'}^2)^2 B_0(p^2, M_{\sigma'}^2, m_K^2)]$$
$$+ \frac{i2\sqrt{2}c_d c_m}{F_0^3 M_S^2 p^2} p_\nu m_K^2 M_{\sigma'}^2 [(m_K^2 + p^2 - M_{\sigma'}^2)B_0(p^2, M_{\sigma'}^2, m_K^2) + A_0(M_{\sigma'}^2) - A_0(m_K^2)], \tag{C33}$$

$$T^{K-cS4} = 2T^{K-cS3} = \frac{-i\sqrt{2}c_d^2}{F_0^3 p^2} p_\nu [(3p^2 + m_K^2 - M_a^2)A_0(M_a^2) - (p^2 + m_K^2 - M_a^2)A_0(m_K^2) + (p^2 + m_K^2 - M_a^2)^2 B_0(p^2, M_a^2, m_K)]$$
$$+ \frac{i2\sqrt{2}c_d c_m}{F_0^3 M_S^2 p^2} p_\nu m_K^2 M_a^2 [(m_K^2 + p^2 - M_a^2)B_0(p^2, M_a^2, m_K^2) + A_0(M_a^2) - A_0(m_K^2)], \tag{C34}$$

$$T^{K-cS6} = 2T^{K-cS5} = \frac{-i\sqrt{2}c_d^2}{F_0^3 p^2} p_\nu [(3p^2 + m_\pi^2 - M_\kappa^2)A_0(M_\kappa^2) - (m_\pi^2 + p^2 - M_\kappa^2)A_0(m_\pi^2) + (m_\pi^2 + p^2 - M_\kappa^2)^2 B_0(p^2, M_\kappa^2, m_\pi^2)]$$
$$+ \frac{i2\sqrt{2}c_d c_m}{F_0^3 M_S^2 p^2} p_\nu \{[m_K^2 M_\kappa^2 - (m_K^2 - m_\pi^2)(M_\kappa^2 - s - m_\pi^2)]A_0(M_\kappa^2) + [-m_K^2 M_\kappa^2 - (m_K^2 - m_\pi^2)(m_\pi^2 - s - M_\kappa^2)]A_0(m_\pi^2)$$
$$+ [m_K^2 M_\kappa^2 (s + m_\pi^2 - M_\kappa^2) - (m_K^2 - m_\pi^2)(s^2 - M_\kappa^4 - m_\pi^4 + 2m_\pi^2 M_\kappa^2)]B_0(p^2, M_\kappa^2, m_\pi^2)\}$$
$$+ \frac{i2\sqrt{2}c_m^2}{F_0^3 M_S^4 p^2} p_\nu \left\{ \left[-m_K^2 (m_K^2 - m_\pi^2) M_\kappa^2 - \frac{(m_K^2 - m_\pi^2)^2}{2}(m_\pi^2 - s - M_\kappa^2) \right] A_0(M_\kappa^2) \right.$$
$$+ \left[m_K^2 (m_K^2 - m_\pi^2)(2s + M_\kappa^2) - \frac{(m_K^2 - m_\pi^2)^2}{2}(3s + M_\kappa^2 - m_\pi^2) \right] A_0(m_\pi^2)$$
$$\left. + \left[m_K^2 (m_K^2 - m_\pi^2)(s + M_\kappa^2 - m_\pi^2) M_\kappa^2 - \frac{(m_K^2 - m_\pi^2)^2}{2}(s + M_\kappa^2 - m_\pi^2)^2 \right] B_0(p^2, M_\kappa^2, m_\pi^2) \right\}, \tag{C35}$$

$$T^{K-cS7} = \frac{(c_\theta + 2\sqrt{2}s_\theta)^2}{6} \times \frac{-i\sqrt{2}c_d^2}{F_0^3 p^2} p_\nu [(3p^2 + m_\eta^2 - M_\kappa^2)A_0(M_\kappa^2) - (m_\eta^2 + p^2 - M_\kappa^2)A_0(m_\eta^2) + (m_\eta^2 + p^2 - M_\kappa^2)^2 B_0(p^2, M_\kappa^2, m_\eta^2)]$$
$$+ \frac{i\sqrt{2}c_d c_m}{F_0^3 M_S^2 p^2} p_\nu (c_\theta + 2\sqrt{2}s_\theta) \left\{ \left[\frac{c_\theta + 2\sqrt{2}s_\theta}{3} m_K^2 M_\kappa^2 + c_\theta (m_K^2 - m_\pi^2)(M_\kappa^2 - s - m_\eta^2) \right] A_0(M_\kappa^2) \right.$$
$$+ \left[-\frac{c_\theta + 2\sqrt{2}s_\theta}{3} m_K^2 M_\kappa^2 + c_\theta (m_K^2 - m_\pi^2)(m_\eta^2 - s - M_\kappa^2) \right] A_0(M_\eta)$$
$$\left. + \left[\frac{c_\theta + 2\sqrt{2}s_\theta}{3} m_K^2 (s + m_\eta^2 - M_\kappa^2) M_\kappa^2 + c_\theta (m_K^2 - m_\pi^2)(s^2 - m_\eta^4 - M_\kappa^4 + 2m_\eta^2 M_\kappa^2) \right] B_0(p^2, M_\kappa^2, m_\eta^2) \right\}$$
$$- \frac{i\sqrt{2}c_m^2}{F_0^3 M_S^4 p^2} p_\nu \left\{ \left[-c_\theta (c_\theta + 2\sqrt{2}s_\theta) m_K^2 (m_K^2 - m_\pi^2) M_\kappa^2 + \frac{3}{2} c_\theta^2 (m_K^2 - m_\pi^2)^2 (m_\eta^2 - s - M_\kappa^2) \right] A_0(M_\kappa^2) \right.$$
$$+ \left[c_\theta (c_\theta + 2\sqrt{2}s_\theta) m_K^2 (m_K^2 - m_\pi^2)(2s + M_\kappa^2) + \frac{3}{2} c_\theta^2 (m_K^2 - m_\pi^2)^2 (3s + M_\kappa^2 - m_\eta^2) \right] A_0(M_\eta)$$
$$\left. + \left[c_\theta (c_\theta + 2\sqrt{2}s_\theta) m_K^2 (m_K^2 - m_\pi^2)(s + M_\kappa^2 - m_\eta^2) M_\kappa^2 + \frac{3}{2} c_\theta^2 (m_K^2 - m_\pi^2)^2 (s + M_\kappa^2 - m_\eta^2)^2 \right] B_0(p^2, M_\kappa^2, m_\eta^2) \right\}, \tag{C36}$$

$$T^{K-cS8}=\frac{(2\sqrt{2}c_\theta-s_\theta)^2}{6}\times\frac{-i\sqrt{2}c_d^2}{F_0^3p^2}p_\nu[(3p^2+m_{\eta'}^2-M_\kappa^2)A_0(M_\kappa^2)-(m_{\eta'}^2+p^2-M_\kappa^2)A_0(m_{\eta'}^2)+(m_{\eta'}^2+p^2-M_\kappa^2)^2B_0(p^2,M_\kappa^2,m_{\eta'}^2)]$$
$$-\frac{i\sqrt{2}c_dc_m}{F_0^3M_S^2p^2}(2\sqrt{2}c_\theta-s_\theta)p_\nu\left\{\left[\frac{s_\theta-2\sqrt{2}c_\theta}{3}m_K^2M_\kappa^2+s_\theta(m_K^2-m_\pi^2)(M_\kappa^2-s-m_{\eta'}^2)\right]A_0(M_\kappa^2)\right.$$
$$+\left[-\frac{s_\theta-2\sqrt{2}c_\theta}{3}m_K^2M_\kappa^2+s_\theta(m_K^2-m_\pi^2)(m_{\eta'}^2-s-M_\kappa^2)\right]A_0(M_{\eta'})$$
$$\left.+\left[\frac{s_\theta-2\sqrt{2}c_\theta}{3}m_K^2(s+m_{\eta'}^2-M_\kappa^2)M_\kappa^2+s_\theta(m_K^2-m_\pi^2)(s^2-m_{\eta'}^4-M_\kappa^4+2m_{\eta'}^2M_\kappa^2)\right]B_0(p^2,M_\kappa^2,m_{\eta'}^2)\right\}$$
$$-\frac{i\sqrt{2}c_m^2}{F_0^3M_S^4p^2}p_\nu\left\{\left[-s_\theta(s_\theta-2\sqrt{2}c_\theta)m_K^2(m_K^2-m_\pi^2)M_\kappa^2+\frac{3}{2}s_\theta^2(m_K^2-m_\pi^2)^2(m_{\eta'}^2-s-M_\kappa^2)\right]A_0(M_\kappa^2)\right.$$
$$+\left[s_\theta(s_\theta-2\sqrt{2}c_\theta)m_K^2(m_K^2-m_\pi^2)(2s+M_\kappa^2)+\frac{3}{2}s_\theta^2(m_K^2-m_\pi^2)^2(3s+M_\kappa^2-m_{\eta'}^2)\right]A_0(M_{\eta'})$$
$$\left.+\left[s_\theta(s_\theta-2\sqrt{2}c_\theta)m_K^2(m_K^2-m_\pi^2)(s+M_\kappa^2-m_{\eta'}^2)M_\kappa^2+\frac{3}{2}s_\theta^2(m_K^2-m_\pi^2)^2(s+M_\kappa^2-m_{\eta'}^2)^2\right]B_0(p^2,M_\kappa^2,m_{\eta'}^2)\right\}. \quad \text{(C37)}$$

For the vector resonances, we find that T^{K-cVi} is directly related to the self-energy function Σ^{K-Vi} through

$$T^{K-cVi}=-\sqrt{2}F_0p_\nu\frac{1}{p^2}\Sigma^{K-cVi},\quad i=1,2,3,4,5,6,7,8. \quad \text{(C38)}$$

[1] S. Aoki *et al.*, arXiv:1310.8555; http://itpwiki.unibe.ch/flag.
[2] V. Bernard, M. Oertel, E. Passemar, and J. Stern, Phys. Lett. B **638**, 480 (2006).
[3] S. Weinberg, Physica (Amsterdam) **96A**, 327 (1979).
[4] J. Gasser and H. Leutwyler, Ann. Phys. (N.Y.) **158**, 142 (1984); Nucl. Phys. **B250**, 465 (1985).
[5] J. Bijnens and I. Jemos, Nucl. Phys. **B854**, 631 (2012).
[6] G. Colangelo *et al.*, Eur. Phys. J. C **71**, 1695 (2011).
[7] G. Ecker, J. Gasser, A. Pich, and E. De Rafael, Nucl. Phys. **B321**, 311 (1989).
[8] G. 't Hooft, Nucl. Phys. **B72**, 461 (1974); **B75**, 461 (1974); E. Witten, Nucl. Phys. **B160**, 57 (1979).
[9] J. J. Sanz-Cillero, Phys. Rev. D **70**, 094033 (2004).
[10] J. J. Sanz-Cillero and J. Trnka, Phys. Rev. D **81**, 056005 (2010).
[11] A. Pich, I. Rosell, and J. J. Sanz-Cillero, J. High Energy Phys. 01 (2007) 039.
[12] A. Pich, I. Rosell, and J. J. Sanz-Cillero, J. High Energy Phys. 02 (2011) 109; A. Pich, I. Rosell, and J. J. Sanz-Cillero J. High Energy Phys.07 (2008) 014.
[13] I. Rosell, J. J. Sanz-Cillero, and A. Pich, J. High Energy Phys. 08 (2004) 042.
[14] O. Catà and S. Peris, Phys. Rev. D **65**, 056014 (2002).
[15] C. Davies and P. Lepage, AIP Conf. Proc. **717**, 615 (2004).
[16] C. T. H. Davies *et al.* (HPQCD and UKQCD and MILC and Fermilab Lattice Collaborations), Phys. Rev. Lett. **92**, 022001 (2004).
[17] Y. Aoki *et al.* (RBC and UKQCD Collaborations), Phys. Rev. D **83**, 074508 (2011).
[18] R. Arthur *et al.* (RBC and UKQCD Collaborations), Phys. Rev. D **87**, 094514 (2013).
[19] S. Dürr, Z. Fodor, C. Hoelbling, S. D. Katz, S. Krieg, T. Kurth, L. Lellouch, T. Lippert, A. Ramos, and K. K. Szabó, Phys. Rev. D **81**, 054507 (2010).
[20] J. Soto, P. Talavera, and J. Tarrus, Nucl. Phys. **B866**, 270 (2013).
[21] G. Amoros, J. Bijnens, and P. Talavera, Nucl. Phys. **B568**, 319 (2000).
[22] G. Ecker, P. Masjuan, and H. Neufeld, Eur. Phys. J. C **74**, 2748 (2014).
[23] J. Bijnens and J. Relefors, arXiv:1402.1385; C. T. Sachrajda and G. Villadoro, Phys. Lett. B **609**, 73 (2005).
[24] G. Colangelo and S. Durr, Eur. Phys. J. C **33**, 543 (2004).
[25] T. Feldmann, Int. J. Mod. Phys. A **15**, 159 (2000).
[26] R. Kaiser and H. Leutwyler, Eur. Phys. J. C **17**, 623 (2000).
[27] Z.-H. Guo and J. J. Sanz-Cillero, Phys. Rev. D **79**, 096006 (2009).
[28] J. R. Pelaez, M. R. Pennington, J. Ruiz de Elvira, and D. J. Wilson, Phys. Rev. D **84**, 096006 (2011).
[29] Z.-H. Guo and J. A. Oller, Phys. Rev. D **84**, 034005 (2011).
[30] Z.-H. Guo, J. A. Oller, and J. Ruiz de Elvira, Phys. Lett. B **712**, 407 (2012).
[31] Z.-H. Guo, J. A. Oller, and J. Ruiz de Elvira, Phys. Rev. D **86**, 054006 (2012).

[32] L. Y. Dai, X. G. Wang, and H. Q. Zheng, Commun. Theor. Phys. **57**, 841 (2012).
[33] L. -Y. Dai, X.-G. Wang, and H.-Q. Zheng, Commun. Theor. Phys. **58**, 410 (2012).
[34] Z.-Y. Zhou and Z. Xiao, Phys. Rev. D **83**, 014010 (2011).
[35] F. Ambrosino *et al.*, J. High Energy Phys. 07 (2009) 105.
[36] I. Rosell, P. Ruiz-Femenia, and J. Portolés, J. High Energy Phys. 12 (2005) 020.
[37] J. J. Sanz-Cillero, Phys. Lett. B **681**, 100 (2009).
[38] L. Y. Xiao and J. J. Sanz-Cillero, Phys. Lett. B **659**, 452 (2008); A. Pich, I. Rosell, and J. J. Sanz-Cillero, J. High Energy Phys. 01 (2014) 157.
[39] J. Bijnens, E. Gamiz, E. Lipartia, and J. Prades, J. High Energy Phys. 04 (2003) 055; M. Golterman and S. Peris, Phys. Rev. D **74**, 096002 (2006); P. Masjuan and S. Peris, J. High Energy Phys. 05 (2007) 040.
[40] V. Cirigliano, G. Ecker, H. Neufeld, and A. Pich J. High Energy Phys. 06 (2003) 012.
[41] V. Cirigliano, G. Ecker, M. Eidemuller, Roland Kaiser, A. Pich and J. Portolés, Nucl. Phys. **B753**, 139 (2006).
[42] G. Ecker, J. Gasser, H. Leutwyler, A. Pich, and E. de Rafael, Phys. Lett. B **223**, 425 (1989).
[43] I. Rosell, P. Ruiz-Femenia, and J. J. Sanz-Cillero, Phys. Rev. D **79**, 076009 (2009).
[44] M. Jamin, J. A. Oller, and A. Pich, Nucl. Phys. **B622**, 279 (2002).
[45] T. Fuchs, J. Gegelia, G. Japaridze, and S. Scherer, Phys. Rev. D **68**, 056005 (2003).
[46] C. B. Lang, D. Mohler, S. Prelovsek, and M. Vidmar, Phys. Rev. D **84**, 054503 (2011).
[47] S. Aoki *et al.* (CS Collaboration), Phys. Rev. D **84**, 094505 (2011).
[48] C. Pelissier and A. Alexandru, Phys. Rev. D **87**, 014503 (2013).
[49] J. J. Dudek, R. G. Edwards, and C. E. Thomas, Phys. Rev. D **87**, 034505 (2013).
[50] R. Baron *et al.* (ETM Collaboration), J. High Energy Phys. 08 (2010) 097.
[51] C. Michael, K. Ottnad, and C. Urbach, arXiv:1311.5490.
[52] C. Michael, K. Ottnad, and C. Urbach, Phys. Rev. Lett. **111**, 181602 (2013).
[53] N. H. Christ, C. Dawson, T. Izubuchi, C. Jung, Q. Liu, R. D. Mawhinney, C. T. Sachrajda, A. Soni, and R. Zhou, Phys. Rev. Lett. **105**, 241601 (2010).
[54] J. J. Dudek, R. G. Edwards, B. Joo, M. J. Peardon, D. G. Richards, and C. E. Thomas, Phys. Rev. D **83**, 111502 (2011).
[55] E. B. Gregory, A. C. Irving, C. M. Richards, and C. McNeile (UKQCD Collaboration), Phys. Rev. D **86**, 014504 (2012).
[56] Z. H. Guo, J. J. Sanz Cillero, and H. Q. Zheng, J. High Energy Phys. 06 (2007) 030.
[57] Z.-H. Guo, Phys. Rev. D **78**, 033004 (2008).
[58] Z.-H. Guo and P. Roig, Phys. Rev. D **82**, 113016 (2010).
[59] J. Beringer *et al.* (Particle Data Group Collaboration), Phys. Rev. D **86**, 010001 (2012).
[60] Rafel Escribano, Pere Masjuan, and Juan José Sanz-Cillero, J. High Energy Phys. 05 (2011) 094.
[61] S. Descotes-Genon, L. Girlanda, and J. Stern, J. High Energy Phys. 01 (2000) 041.
[62] G. Ecker, P. Masjuan, and H. Neufeld, Phys. Lett. B **692**, 184 (2010).
[63] M. Jamin, J. A. Oller, and A. Pich, Nucl. Phys. **B587**, 331 (2000).
[64] K. Kawarabayashi and M. Suzuki, Phys. Rev. Lett. **16** (1966) 255; Riazuddin and Fayyazuddin, Phys. Rev. **147**, 1071 (1966).
[65] V. Bernard, S. Descotes-Genon, and G. Toucas, J. High Energy Phys. 01 (2011) 107.